Technical Report 4—83

LUNAR SOIL SIMULANT STUDY
Phase B
PART II — THERMAL CONDUCTIVITY

by

J. H. Hubbard

E. S. Gall

H. S. Kahn

May 1969

DEPARTMENT OF THE ARMY

OHIO RIVER DIVISION LABORATORIES, CORPS OF ENGINEERS

Cincinnati, Ohio 45227

The contents of this report are not to be used for advertising, publication, or promotional purposes. Citation of trade names does not constitute an official indorsement or approval of the use of such commercial products. The findings of this report are not to be construed as an official Department of the Army position, unless so designated by other authorized documents.

Destroy this report when it is not longer needed.
Do not return it to the originator

SUMMARY

This report presents the results of an investigation into the thermal conductivity of a Lunar Soil Simulant at pressure levels of 5×10^{-5} torr and below. Thermal measurements were completed in vacuum over the temperature range of 200° K to 425° K. The Lunar Soil Simulant consisted of quarried diabase rock crushed and processed to the gradation of a fine sand. Four distinct combinations of the size fractions of this material permitted evaluation of the effect of grain size on the measurement of thermal conductivity within the sample container. This experimental data was correlated with data obtained by other investigations.

PREFACE

The investigation reported herein was authorized by the Chief of Engineers (ENGMC-EX) in a letter dated 24 May 1966, subject, "Lunar Soil Simulant Work Statement."

The work was performed in the Applied Physics Branch of the Construction Engineering Laboratory, Ohio River Division Laboratories (ORDL). Personnel actively engaged in planning, testing and analysis were Messrs. J. H. Hubbard, E. S. Gall, L. F. Doty, R. T. Neu, and M. M. Powell and Mrs. H. S. Kahn. This report was prepared by Messrs. J. H. Hubbard and E. S. Gall and Mrs. H. S. Kahn. The Director and Assistant Director of the Ohio River Division Laboratories during this study were Messrs. F. M. Mellinger and R. L. Hutchinson, respectively.

Special acknowledgement is given to Drs. P. E. Glaser and A. E. Wechsler of the Arthur D. Little and Co. for their valuable guidance and encouragement in interpreting and assessing the experimental work. Dr. L. F. Doty of the University of Cincinnati was a great help in the mathematical analysis of the data.

CONTENTS

CONTENTS (cont)

TABLES

PLATES

FIGURES

LUNAR SOIL SIMULANT STUDY, PHASE B

PART II - - THERMAL CONDUCTIVITY

PART I: INTRODUCTION

Background

1. A study to develop a lunar soil simulant whose physical behavior in the earth's gravity field approximates the assumed behavior of a lunar soil in the reduced gravity field of the moon was initiated in Fiscal Year 1966. The study was divided into three parts. The first part (Phase A) of the study has been completed and was reported on in April 1966 (1)*. The purpose of this Phase A was to develop a material, designated Type A Lunar Soil Simulant, which would have certain prescribed properties when placed in an environment varying in pressure from one atmosphere to 10 torr. The lunar simulant was derived from unweathered diabase rock crushed and processed so as to fall within the gradation band shown in Figure 1. Other physical properties of the Type A Lunar Soil Simulant determined during Phase A include:

a. Bulk density (free fall state) - 1370-1450 kg/m^3
b. Particle specific gravity - 3.02-3.16
c. Light reflectivity (albedo)-0.07-0.09%
d. Sinkage under a pressure 3.45N/cm^2 - 2.5-5.0 cm
e. Thermal conductivity (k) (in air) 4.19×10^{-3} watts/cm°C.

2. The thermal conductivity for Phase A was measured in an apparatus consisting of coaxial aluminum cylinders. Heat was introduced from a rod heater, placed inside the inner cylinder, and was dissipated through the air-cooled outer cylinder. Temperature measurements at two different radii determined the radial temperature gradient.

Purpose and Scope

3. The purpose of this investigation (Phase B, Part 2) was to determine the thermal conductivity of the lunar soil simulant at an ambient pressure of 10^{-5}

* Parenthetic numbers indicate references.

torr. Thermal conductivity was to be measured over the range of 200°K to 425°K. The effects of particle size and gradation of the simulant material were to be investigated by making comparative measurements on the simulant with its specified gradation, on the -100 mesh and +100 mesh fractions, and on a well-graded sample of simulant material. The results reported herein constitute the final part of the Phase B study. The experimental data for the -100 mesh gradation fraction was analyzed in detail. Experimental data from the other three gradation fractions was tabulated but not analyzed in detail.

Approach

4. The high vacuum facility available at these Laboratories provided the required ambience under which the measurement of the thermal conductivity of the simulant was completed. Simulant cooling to the low temperatures stipulated in the sponsor's work statement required a liquid nitrogen heat sink. A more detailed description of the experimental apparatus appears in paragraphs 10 through 17.

5. The primary effort of this study was the measurement of thermal conductivity in one selected fraction prepared from the Type A Lunar Soil Simulant. The design of the experimental apparatus chosen for the thermal measurements used the line heat source principle. The line heat source method measures the temperature rise at a point caused by controlled heat input into a small heating wire. This method is ideally suited to fine grained sands or powders because the wires comprising the heart of the apparatus are of comparable size to the surrounding particles. The apparatus is also suitable for use in a vacuum environment because it is simple to construct and requires a small sample volume. The small volume is advantageous because the small quantities of material (1) allow changes in sample temperature to be made in a reasonable time and (2) reduce the time required to outgas the sample material.

PART II: EQUIPMENT AND TEST APPARATUS

High Vacuum Facility

6. The high vacuum facility (Plate 1) consists of three major components: forepump, diffusion pump, and working chamber. The mechanical forepump, rated at 7.1 liters per second, (15 cfm), provides initial or rough pumping down to a pressure of about 10^{-2} torr. At this pressure, a pneumatically-operated gate valve is opened to permit the diffusion pump to operate in its most efficient environment. The 15-cm (6-in) oil diffusion pump with a nominal pumping speed of 1440 liters per second (3050 cfm) will attain pressures into the 10^{-6} torr range with the experimental apparatus in place. A water-cooled chevron baffle installed at the throat of the system reduced backstreaming of diffusion pump oil into the working chamber. The working chamber consists of a 46-cm (18-in) stainless steel feed through collar surmounted by a 46-cm (18-in) diameter by 46-cm (18-in) high pyrex bell jar. A butyl rubber gasket provides the principle bell jar seal. The heat sink required by the condition of test consists of an aluminum reservoir supplied with liquid nitrogen by means of a dual line cryogenic feedthrough (Figure 5).

Pressure Measurements

7. Three gauges measured the pressure in the system:

a. The thermocouple gauge placed in the roughing line provided readings in the roughing range and indicated when the diffusion pump could be placed into the system.

b. A cold cathode ionization gauge provided pressure measurement capability down to the mid 10^{-7} torr range. Mounting the gauge in the throat section between the working chamber and the chevron baffle resulted in pressure readings somewhat lower than the actual pressure in the working area.

c. An NRC Alphatron gauge, mounted on the feedthrough collar, provided readings of pressure in the working chamber from atmosphere down to the mid 10^{-4} torr range. It was used to monitor the chamber pressure for test runs below -40 ^{o}C.

Description of Simulant Test Material

8. The Type A Lunar Soil Simulant created during Phase A of this study provided the material for the preparation of four test specimens of differing gradations. Figure 2 presents the gradation curves for each of the separated fractions. An analytical sieving device separated each test specimen in a nest of sieves to provide the data needed to plot each grain size distribution curve. The gradation fractions selected were intended to provide a wide range of grain size distributions so as to evaluate the effect of the larger particles on the measurement of thermal conductivity. The designation and description of the four fractions are:

a. Type A: the Lunar Soil Simulant prepared in the first part (Phase A) of the study.

b. Type A-1: that portion of the Type A simulant passing the No. 100 sieve.

c. Type A-2: that portion of the Type A simulant with 80% retained on the No. 140 sieve.

d. Type A-3: that portion of the Type A simulant proportioned so as to fall within the allowable limits of fine concrete aggregate (ASTM specification No. C 33-66).

Photomicrographs

9. The photomicrographs presented on Plate 2 show the angular shape of some individual grains of the Type A-1 fraction. The photographs were selected from a series taken with a 35 mm Kodak Retina S camera mounted directly to a Bausch and Lomb microscope. The nominal magnifying power of combined objective and oculars was 20 x and 40 x, respectively. The small scale divisions in each photograph are 0.01 mm or 10 microns apart. Dual illumination permitted simultaneous recording of the back lighted scale and oblique lighted simulant grains.

Test Set Up for Measurement of Thermal Conductivity of Materials

10. Figure 3 shows the overall dimensions of the test container as well as a detail of the end plates. Aluminum was used throughout except for the steel set

screws, and pins, and the teflon thermal isolation insert. The thermal isolation inserts were machined to a stepped configuration from teflon and press fitted into holes drilled in the center of the end plates. The set screws forced the plates to slide on the aligning pins thus applying axial motion to straighten the embedded wires for initial alignment.

11. Mounting the three wires in the test container required great care. Each wire was fed through small tubes pressed into guide holes drilled in the teflon inserts. A bead of solder larger than the guide holes provided the reaction for tightening the wires. When the wires were in place, one of the jacking plates was backed off until the wires appeared taut under approximately equal tension. The lead wires were soldered to an amphenol connector which slipped over the pins of an eight wire electrical feed through mounted in the vacuum system collar. After unplugging the connector, the test container was removed from the working chamber and set on a table. The simulant material was then carefully spooned into the container and the top surface was leveled by screeding.

12. The line heat source apparatus consisted of three small wires arrayed horizontally along the length of a rectangular box in which the material was placed at a preselected density. The wires were positioned in the box through guide holes set at the center of the ends. Figure 4 shows the spatial relationship of the three wires in the box. The central wire of the set was the constantan heater wire. The wires on either side were copper or constantan leading to the thermocouple junctions. Each wire was nominally 0.003 inches (7.62×10^{-3}cm) in diameter. The thermocouple junction consisted of a disc 0.003 inches (7.62×10^{-3}cm) thick by approximately 0.035 inches (8.89×10^{-2}cm) in diameter. The thermocouples were installed approximately 0.10 inches (0.254 cm) on either side of the heater wire. A more complete treatment of the assumptions inherent in the apparatus and the potential errors in the apparatus are presented in Appendix A.

13. Heat was generated in the apparatus by impressing constant voltage across the heater wire from a d. c. power supply. A Leeds and Northrup millivolt potentiometer attached to the lead wires of each thermocouple measured the absolute temperature at each junction. The test schedule called for readings every five minutes over the duration of the test run. The thermocouples were read separately within 15 seconds of each time unit.

Heat Sink

14. In order to reduce the temperature of the test samples, it was necessary to use a liquid nitrogen heat sink. The heat sink apparatus consisted of a vacuum-

tight reservoir into which liquid nitrogen could be fed. The reservoir consisted of an extruded aluminum rectangular tube closed at the ends with heliarc welded aluminum plates (Figure 5). Two short lengths of 1/4-inch (0.635-cm) diameter aluminum tubing were heliarc welded to one of the plates. Additional tubing coupled to the short lengths, extended to a stainless steel dual line cryogenic feedthrough installed on the feedthrough collar. Torr Seal, a low vapor pressure epoxy system, was applied to the weldments to eliminate real gas leaks. Liquid nitrogen from a supply dewar entered the apparatus through a braided copper transfer line coupled to one of the lines of the cryogenic feedthrough. The liquid nitrogen then flowed to the reservoir where it formed a pool with a depth of about 20 mm. Excess liquid or gaseous nitrogen escaped to atmosphere through the other line.

15. Because the thermal conductivity of the evacuated simulant was very low, the length of time required to lower the temperature of a test sample to the extreme low temperatures required by the investigation could be very long. It was found that the time required to cool could be significantly reduced by introducing convective transfer of heat as well as grain to grain conduction. The convective process was introduced after the chamber had been pumped down and after liquid nitrogen had been introduced into the reservoir. At this point, the working chamber was isolated by closing the pneumatic valve, and dry nitrogen was bled into the chamber. The nitrogen, cooled by the reservoir, permeated the sample and allowed convection to occur. A soaking period of an hour in the nitrogen atmosphere provided ample opportunity for the temperature in the simulant to reduce to the order of 125°K.

16. Because the test container rested directly on the top surface of the heat sink reservoir, heat transfer - even with the convention capability of soaking at roughing pressure - was not wholly satisfactory. Heat transferred from simulant to reservoir primarily through the walls of the test container. The possibility existed then that as the aluminum boundaries around the sample were cooled, the very low thermal conductivity of the simulant would result in significant temperature gradients within the sample. A series of temperature probe measurements revealed the extent of this gradient for very low temperatures. These measurements showed a relatively linear temperature distribution in the sample. A typical set of temperature readings are shown by Figure 6.

17. A basic assumption of the line heat source equation used in data analysis is that the observed temperature rise emanates from a constant environment. Paragraphs 68 through 75 of Appendix A show that a constant environment need not imply a uniform temperature field. The analysis of initial temperature distribution in the Appendix shows that computations of thermal conductivity are not affected by an initial linear temperature distribution.

Simulant Preheating

18. Simulant preheating was shown to be beneficial in the initial part of the Phase B study. A report (2) showed that if the simulant were heated to temperatures above 423°K for a period of at least 24 hours, evacuation of the material was rapid and no geysering occurred. A single filling of the test container with heated material sufficed to give an indication of variation of thermal conductivity over the complete range of temperatures. The initial placement conditions were duplicated for additional tests.

Simulant Handling

19. After unplugging the amphenol connector, the test container was removed from the working chamber and set on a table. The heated material was then carefully spooned into the container so as to avoid displacement of the three wires. Careful screeding of the top surface insured that each test was completed with the same volume of material. The densities achieved for each gradation fraction were:

Gradation Fraction	Density (kg/m^3)
Type A	1450
Type A-1	1350
Type A-2	1540
Type A-3	1525

20. Hot air driven from a heat gun raised the temperature of the test container to approximately the simulant temperature before placement of the simulant. Transfer of the hot container into the working chamber was completed as quickly as possible after the sample had been screeded. Although pumping started with a minimum of delay, some heat loss did occur. This amounted to between 15 and 25°C depending upon gradation fraction and handling time.

21. Some vibration during a test was unavoidable. The primary source of vibration lay in the process of cooling. The transfer of liquid nitrogen to the heat sink reservoir included an initial violent gaseous phase as well as the more quiescent pool phase during which heat flowed from the sample. The initial phase flexed the aluminum tubes cantilevered into the working chamber from the cryogenic feedthrough (Figure 5). This random flexing shook both the reservoir and test container, thus inducing some densification to the sample. The increase in density, however, is not as significant to thermal conductivity measurements as the altered conduction path created by the rearrangement of the simulant grains.

PART III: TEST PROCEDURE

22. The first stage of the test procedure was identical for each gradation fraction and consisted of material preheating, placement in test container, and evacuation in the vacuum chamber. With the exception of the test runs at very low initial temperature, the pressure level reached at the start of each thermal test was on the order of 5×10^{-5} torr. The tests performed to define thermal properties at temperatures below about 230°K required special handling as described in paragraph 24.

23. The second stage of testing occurred after the creation of the vacuum environment and after establishing a stable temperature in the material. This stage consisted of impressing three volts across the heater wire and monitoring the temperature at the two thermocouple stations. Thermocouple readings to the nearest half degree Celsius continued at five-minute intervals for the 90-minute duration of the test. Subsequent test runs were made after significant reduction in simulant temperature. Test runs on material below room temperature required liquid nitrogen cooling but followed the same basic procedure.

24. In order to determine thermal conductivity for the very low temperatures (200°K to 235°K), it was necessary to reduce the temperature in the simulant to about 150°K. This was done by the soaking technique described in paragraph 15. It was not practical to impress three volts across the heater wire because the resulting temperature rise was rapid (on the order of 50°C during the initial five-minute observation period) and the shape of the temperature-time curve was too uncertain for analysis. Reducing the impressed voltage to 1.5 to 2 volts resulted in a slower rate of rise and thus permitted a more reliable analysis.

Data Analysis

25. When a line source of heat generates into an infinite volume of material, the resulting temperature field is cylindrical. The temperature rise at any point in the material is a function of the heat input, the distance to the source and the thermal properties of the material (3).

These quantities are related by:

$$T = \left(\frac{-q}{4\pi k}\right) \quad Ei\left(\frac{-r^2}{4\alpha t}\right) \tag{1}$$

where:

T = the temperature (^{o}Kelvin)

q = heat flux per unit length (cal/cm sec)

k = coefficient of thermal conductivity (cal/cm sec ^{o} C)

r = radial distance from line heat source (cm)

α = thermal diffusivity ($k/\rho c$) of the media (cal cc/g cm sec ^{o}C)

ρ = density of the media (g/cc)

c = specific heat of the media (cal/gm ^{o}C)

Ei(x) = exponential integral of x, $\int_x^{\infty} \frac{e^{-x}}{x} dx$

26. If the quantity ($\frac{r^2}{4\alpha t}$) is less than an arbitrary value of 0.03[3], the following approximation of Equation (1) holds:

$$T = - \frac{q}{4\pi k} \left[0.5772 + \text{Ln} \frac{r^2}{4\alpha t} \right] \qquad (2)$$

For the experiments considered in this report, typical values of the parameters comprising the quantity ($\frac{r^2}{4\alpha t}$) were:

r = 0.2 cm

k = 7.5×10^{-6} cal/cm sec ^{o}C

ρ = 1.5 gm/cc

c = 0.2 (cal/gm ^{o}C)

For the geometry of the line heat source apparatus, the quantity ($r^2/4\alpha t$) will be less than 0.03 only for times greater than about 180 minutes. Therefore, the approximation presented in Equation (2) could not be applied within an economical time frame.

27. Two analytical approaches were examined for reducing the experimental data. Both methods were derived from Equation 1 and used the experimental temperature vs. time plot (Figure 7). The first approach applied a curve fitting procedure to the experimental curve and found the slope of each curve over a 15-minute time interval defined by the temperature range of interest. (This technique is explained in detail in Appendix B.) Although mathematically precise, the method was found to be impractical for this work because of the involved nature of the calculations. The experimental points described a curve too close to linear for effective fit with a parabola.

28. The method of choice was the curve-matching technique discussed by Wechsler and Simon (4). Equation 1 Indicates that the temperature rise at any point in the sample is a function of the heat flux, the thermal conductivity and a generalized function Ei (X). For convenience, this function may be written in the form $-Ei(-1/X)$, where X is equal to the quantity $(4\pi t/r^2)$. A plot of logarithm temperature rise versus logarithm time from the experimental data should have the same shape as the curve described by plotting logarithm $-Ei(-1/X)$ versus logarithm X (Figure 8 illustrates the technique for a typical set of experimental data points.) To find the conductivity, it is necessary to move the curve Ln versus Ln t parallel with the axes until the experimental curve matches the curve of Ln Ei (-1/X) versus LnX at a value of $-Ei(-1/X)$ equal to unity. The temperature, T*, associated with the match, is then entered into the equation:

$$k = q/4\pi\ T^* \qquad (3)$$

The thermal conductivity, k, is therefore uniquely described by the experimental curve.

PART IV: ERROR ANALYSIS

Potential Sources of Experimental Error

29. The mathematical model, used in the analysis of test results, requires certain assumptions about the experimentation which are only partially satisfied. These assumptions fall into three categories:

a. the state of the sample
b. the effect of the boundaries of the container
c. the heat flow to the sample from the line heat source device.

The degree to which these assumptions differed from reality define the error to be anticipated.

Assumptions as to the State of the Sample

30. The first category implies a sample that is a continuum, i. e., absolutely continuous and homogeneous throughout. This assumption cannot be satisfied by a particulate mass consisting of discrete particles. Carefully controlled placement in the container and restricted range in particle size resulted, however, in a reasonable approximation to a continuum. The second assumption of this category states that a constant environment exists during test, i. e., the thermal properties are independent of temperature, temperature gradient, and time.

Assumptions due to Boundary Conditions

31. The second category describes the potential effect of the aluminum container on the temperature distribution within the test sample. The basic assumption is that the boundaries of the container are sufficiently remote from the line heat source device that any thermal gradient set up at the interface of container and simulant will have a negligible effect on the heat transfer between the heater wire and the thermocouples during the measurement period. (Paragraphs 68 through 75 of Appendix A discuss this assumption in detail.)

Assumptions Required by the Line Heat Source Apparatus

32. The final category includes seven assumptions required by the line heat source device itself.

a. The ratio of the heater wire radius to its length is small enough to be considered infinitesimal in establishing the temperature distribution during test.

b. The flow of heat from the heater wire is normal to the axis of the heater and the effect of any non-uniformity of heat output along the wire is negligible.

c. The heat capacity of the heater wire is sufficiently low that the portion of output power used to raise the temperature of the wire is negligible.

d. The length of the heater wire buried in the simulant is long enough to be considered infinite.

e. Any axial heat loss due to conduction along the heater or thermocouple wire does not affect the temperature distribution during testing.

f. Whatever temperature distribution exists at the start of a test run is linear.

g. The responses of the thermocouples are independent of the orientation of the thermocouple junction.

Analysis of Potential Error due to the Assumptions Required in the Experimental Apparatus

33. Each of the assumptions listed above must be critically examined to assess the effectiveness of the testing program. The assumptions noted in paragraph 30 are difficult to evaluate analytically, because of the presence of vibration during test (see paragraph 21). For any given arrangement of particles, the heat path from heater to thermocouple junction should be constant. The path may be circuitous, but so long as the relative positions of the grains are unchanged, the temperature rise at a point in the mass should be repeatable. But the vibration that was present caused an indeterminable amount of particle rearrangement and therefore changed the initial heat path. This effect would be least noticeable for the restricted range of small particles comprising the Type A1 gradation fraction. Because the vibration was primarily due to the introduction of liquid nitrogen, experimental scatter should be more pronounced for the lower temperature runs.

34. The second assumption of paragraph 29 (that the thermal properties are independent of temperature) presents a logical problem that is beyond the scope of existing theory. The results of this study show that thermal conductivity is dependent on temperature. The analysis of results based on the assumption of independence of temperature therefore force an additional assumption; that the thermal conductivity remains essentially constant over the temperature range chosen for each computation.

35. A detailed analysis of the assumption presented in paragraph 31 appears in Appendix A. The very important conclusion of this analysis is that an initial linear temperature distribution in the test material will have no effect on the computation of the thermal conductivity.

36. The first four assumptions of paragraph 32 are satisfied by the geometry of the test device. The relative error due to axial heat loss, however, may be as high as $\pm 3\%$. The assumption of a linear temperature distribution prior to test appears reasonable based on the temperature probe tests discussed in paragraph 16. The final assumption that the orientation of the thermocouple junction had no effect on the thermocouple readings cannot be evaluated. The orientation of the thermocouple junction disc (see paragraph 12) could not be ascertained after the junction was covered with test material. The error due to disc orientation is estimated to be less than $\pm 2\%$. The total estimated error due to the line heat source apparatus should be less than $\pm 5\%$.

Analysis of Error due to Computational Methods

37. The errors inherent in the curve fitting technique are discussed in Appendix B. The conclusions reached are:

1. The approximating curve based on the experimental data may be considered as a smooth curve exactly representing the experimental data.

2. The accuracy of curve fitting is within the time accuracy of recording observations.

3. The error associated with finding the slope of the fit rather than the exact curve is on the order of $\pm 4\%$.

4. The error in computing the thermal conductivity, k, is greatly magnified if the time interval over which computations are made is too small. (See paragraph 84 of Appendix B). A time interval of 15 minutes was found to be optimum considering the implied temperature range of 30°C or less. Because k varies with temperature, the choice of a longer time interval could not be justified.

38. The curve fitting technique presented problems in application that precluded its use. The curve shown in Figure 9 is virtually linear over the 15 minute interval where the curves coincide. Calculation of the coefficients of the parabola required to fit so linear a curve required a keyboard capacity beyond that available to the laboratories. It was therefore decided to adopt a curve matching technique whereby the experimental curves could be moved until a match with a standard curve could be obtained. The accuracy of matching depends upon the judgment of the analyst and cannot be rigorously defined. However, the estimated error in data analysis should be less than $\pm$ 5%.

Analysis of Error due to Instrumentation

39. The instrumentation was checked for both calibration and repeatability. The measuring instruments were determined to be accurate in the ranges used to within reading limitations. The most serious possibility of error of this kind lay in the measurement of power input to the heater wire. Since this enters linearly into the computation of thermal conductivity, the percent error it contributes to the thermal conductivity would be the same as that in the power measurement itself. This was determined to be less than $\pm$ 4%, and the total error due to instrumentation alone was estimated to be less than $\pm$ 5%.

Summary of Error Analysis

40. The error analysis completed for this report examined four major areas:

1. Possible errors due to the assumptions required by the test apparatus.
2. Errors associated with the test boundary conditions.
3. Errors due to data analysis techniques.
4. Errors due to instrumentation.

The error associated with the test boundary condition is believed negligible. The estimated error in each of the remaining three areas should be less than $\pm$ 5%. The combined potential error in measured thermal conductivity should therefore be less than $\pm$ 15%.

PART V: RESULTS

Presentation

41. The results of the thermal conductivity measurements are summarized in Tables 1 through 4. The tables present the results of all tests and are grouped according to gradation fraction. Figure 7 is a typical plot of experimental data. Because the Type A-1 material was most uniform in grain size, it was selected for detailed analysis.

42. Table V summarizes the results of calculations for three models chosen to provide a basis for fitting the data points of the Type A-1 material. Also shown are the results of similar studies on basalt powder as reported by Wechsler and Simon. The table presents the solid conduction and radiative contributions for each material over the temperature range 200°K to 400°K. The bulk density and particle size ranges are also indicated.

43. Figure 10 is a plot of effective thermal conductivity versus temperature for five basalt powders. The two curves indicated by dashes were reproduced from the Wechsler and Simon report. The solid curve represents the fit obtained in this work. Figure 11 repeats the data points for the Type A-1 material but indicates the experimental confidence by the error bars corresponding to the estimated $\pm$ 18% root mean square deviation around the fit curve. It should be noted that the anticipated experimental error ($\pm$ 15%) falls within the error bars indicating the magnitude of scatter attributable to the experiment.

Discussion

44. The flow of heat through a granular material includes three processes of heat transfer: (a) solid conduction from particle to particle, (b) gas conduction in the void spaces of the material and (c) radiation across the void spaces or through the particles (5). Because the tests were conducted at pressures below 5×10^{-5} torr, the contribution of gas conduction to the total heat transfer mechanism was assumed to be negligible.

45. Solid conduction of heat in a granular material occurs through the particles and across the areas of contact of adjacent particles. The effective conductivity is strongly influenced by the interaction of the grain surfaces in the vicinity of the contact points. The flow of heat describes a circuitous path around the voids in the material and will be affected by any change in particle orientation due to change in density.

46. Radiation transfer in the simulant may include the following processes: reflection from a particle surface, transmission through solid or void space, or absorption by the solid particle together with subsequent re-radiation. In general, that portion of the total conductivity traceable to radiation varies as the cube of the mean temperature, emissivity properties of the material and geometrical factors.

Experimental Data Analysis

47. Plots of temperature versus time were prepared for each gradation fraction of the simulant material. The curve matching technique (paragraph 28) was applied to each test run and the resulting thermal conductivity values summarized in Tables 1 through 4. Tables 1, 3 and 4 were not analyzed further because the point scatter indicated experimental uncertainty and a variation that is too erratic to extract a conclusion. The apparently random variation in thermal conductivity for these three gradation fractions was due to the presence of relatively large particles in the test specimen and to the vibration to the test container which occurred as the specimen was cooled. The large grains violate the assumptions of material uniformity and homogeneity implicit in the experimental method (see paragraph 30). Since a significant percentage of the larger particles approach in dimension the distance between heater and thermocouple wires, a strong possibility exists that in some cases a large particle could form a solid bridge between heater wire and thermocouple junction. It is also possible that several large grains could pack in such a way as to form a void around a junction thus decreasing the efficiency of heat transfer from tested material to thermocouple. The problems of bridging and void formation would tend to be much greater for larger size particles than for grains whose maximum dimensions were small compared to the separation between heater and thermocouple wires. Finally, the vibration present during the cool-down process would aggravate the situation because vibration induced motion to the larger particles would change the heat transfer path to a much greater extent than would occur in a test specimen consisting of particles of uniform size.

48. Of all the gradation fractions tested, the Type A-1 lunar soil simulant material most nearly approached the uniformity and homogeneity required by assumption, and was least affected by vibration. Figure 2 shows that approximately 90% of the grains fell within the particle size range 40-149 microns. The results of the thermal conductivity measurements for this material are shown in Table II. The tabulated results indicate that the effective thermal conductivity decreases as the temperature decreases. The consistency of the decrease as well as the overall magnitude of the change indicates that the change is a real effect and not due to errors introduced by experimental procedures or computations.

49. Figure 10 is a plot of effective thermal conductivity versus temperature for the Type A-1 material together with the results of other investigators. The curve through the experimental data points was fit by the least squares method. In order to determine the form of the curve to which to fit the experimental data, it was necessary to consider the contributions of solid conduction and radiation to the effective thermal conductivity of the material. The relative importance of each can be determined by the effect of temperature on the thermal conductivity. The solid conduction contribution in a powder is a function of the particle size, density, applied load, and other factors as well as the thermal conductivity of the solid. The solid conduction contribution, however, is directly proportional to the bulk solid conductivity, which varies with temperature. In glasses, the solid conductivity k_s generally has one of the following forms:

$$k_s = \text{constant} = B'$$

or

$$k_s = B' + C'T$$

In crystalline materials, the conductivity over the temperature range under consideration may have the form:

$$k_s = B' = D'/T$$

50. Thus, the solid conduction factor k_c may have any one of the forms:

$$k_c = F_1 B' = B$$

$$k_c = F_1 (B' + C' T) = B + C T$$

$$k_c = F_1 (B' + D'/T) = B + D/T$$

where F_1 may be considered the constant of proportionality and B, C and D are constants. F_1 is a function of particle size, density, applied loading, etc., but is independent of temperature and of the thermal conductivity of the solid.

51. The radiation contribution k_r to the thermal conductivity is assumed to have the form:

$$k_r = A T^3$$

52. In fitting the curve to the experimental data, three theoretical models were considered, each being representative of the data for appropriate choices of the coefficients. The coefficients were determined by the least squares technique. The models considered were:

$$\text{Model I:} \quad k = B + AT^3 \tag{1}$$
$$\text{Model II:} \quad k = B + CT + AT^3 \tag{2}$$
$$\text{Model III:} \quad k = B + D/T + AT^3 \tag{3}$$

The coefficient of the radiation term A, and the coefficient B should both be positive indicating an increase in thermal conductivity with temperature. On the other hand, the coefficients C and D may be either positive or negative depending on the properties of the material. Positive values of C indicate a conductivity increase with temperature. Positive values of D indicate a flattening of the conductivity-temperature curve.

53. Models I and II represent a powdered glassy material with little or no temperature coefficient of conductivity. Model III should be more representative of a powder prepared from a crystalline material. The least squares technique was applied to each of these equations and the values of the coefficients and the root mean square deviations were calculated. The results of these calculations are:

Model	Equation of Fit	RMS Deviation (%)
I	$k_e = 1.77 \times 10^{-5} + 0.3304 \times 10^{-12} T^3$	18
II	$k_e = 0.98 \times 10^{-4} - 4.69 \times 10^{-7} T + 2.48 \times 10^{-12} T^3$	17
III	$k_e = 17.8 \times 10^{-6} - 16.5 \times 10^{-6}/T + 0.329 \times 10^{-12} T^3$	18

54. In order to evaluate which of the three models best fit the diabase material, the effective conductivity k_e was separated into the radiative contribution (represented by the cubic term) and the solid conduction term. Inspection of the results summarized in Table V indicate that the coefficients obtained for Model II are unreasonable. Over the temperature range 200°K to 400°K, the coefficients obtained for Models I and III are reasonable and, in fact, virtually identical. Model III was chosen because it represents a powder prepared from a crystalline rather than a glassy material and should more nearly approximate the Type A-1 material.

55. When comparing the results of this work to that of other investigators (see Figure 10), it is immediately apparent that the results for the Type A-1 diabase are somewhat higher than the values reported previously. It should be noted that the figure indicates basalts of widely differing composition, particle size and density. Of all the materials reported, the results of Wechsler and Glaser (6) most nearly approximate the Type A-1 material in terms of particle size range and density. These results lie within the 18% error band of the Type A-1 data.

56. The two basalts indicated on Figure 10 by the dashed lines (Wechsler and Simon) are more restricted in grain size and of somewhat greater bulk density. Nevertheless, the shape of the curve fit to the Type A-1 data is very similar except at the higher temperatures.

57. In analyzing these high values, it is necessary to refer to Table V and consider the final three entries. Each material shows a trend of increasing effective conductivity with temperature. The radiative contribution appears to increase as the particle size increases. The solid conduction contribution of the Type A-1 material (Model III) does not follow the trend of decreasing conductivity with increasing particle size. It should be noted that the Type A-1 material embraces a much wider range of particle sizes than do the materials of Wechsler and Simon. The gradation curve for the Type A-1 material (Figure 2) indicates that about 58% of the sample falls between 74 and 149 microns. Approximately 10% of the material is 40 microns or less in greatest dimension. Because these finer particles tend to nestle among the voids between coarser particles, it is reasonable to assume that more contact points and paths are effective in conducting heat than would occur between particles of nearly identical dimensions. This supposition is supported by the generally high results indicated by Wechsler and Glaser. The tendency would be especially evident for the angular particle shape developed in the Type A-1 material during processing (see paragraph 9).

58. Other factors which may help to account for the reported discrepancies include the type of basalt, the processing procedure, the vibration induced densification and the method of preliminary specimen handling.

59. It may be inferred from this discussion that the effective thermal conductivity of the Type A material will not differ significantly from that reported for the Type A-1. However, some increase in the solid conduction term should be expected because of the wider range of particle size.

PART VI: CONCLUSIONS AND RECOMMENDATIONS

Conclusions

60. The inconsistency in the results for the samples containing significant quantities of large grains indicates that the experimental apparatus used was not suitable for measurements on samples containing large particles.

61. The experimental results for the Type A-1 lunar soil simulant demonstrate a strong dependence of the effective thermal conductivity of a granular mineral material on temperature under a vacuum environment.

62. The best fit curve through the experimental data points satisfies the equation:

$$k_e = 17.8 \times 10^{-6} - 16.5 \times 10^{-6}/T + 0.329 \times 10^{-12}\ T^3$$

63. The radiative contribution to the effective thermal conductivity continues the trend reported by others of an increase in thermal conductivity as the particle size increases.

64. The solid conduction contribution does not follow the trend of decreasing conductivity with increasing particle size. This contribution appears to be more strongly influenced by the greater number of contact points and paths developed within a material possessing a wide range of particle sizes.

65. The effective thermal conductivity for the Type A lunar soil simulant should not differ significantly from that reported for the Type A-1 material.

Recommendations

66. It is recommended that work be continued using gradation fractions of the lunar soil simulant with more restricted grain size distributions. This should be done to more precisely define the temperature dependence of thermal conductivity and also the overall dependence on grain size. The range of grain sizes chosen for investigation should be chosen so as to more fully define the radiative and solid conduction contributions to the effective thermal conductivity.

67. It is further recommended that some means, such as an embedded thermocouple or Pirani vacuum gauge, be included in future experiments to monitor pressure within the simulant mass if some readings must be taken at roughing pressure to extend the temperature range considered. This could possibly be done by embedding the vacuum gauge in a test container holding material identical to that whose thermal conductivity is being measured.

REFERENCES

1. J. H. Hubbard, E. S. Gall and D. J. Keller, "The Development of a Lunar Soil Simulant Type A," Ohio River Division Laboratories, Corps of Engineers, Technical Report No. 4-51, April 1966.

2. J. H. Hubbard and E. S. Gall, "Lunar Soil Simulant Study, Phase B: Part I, Outgassing Characteristics," Ohio River Division Laboratories, Corps of Engineers, Technical Report No. 4-58, December 1966 (Draft).

3. John W. Salisbury and Peter E. Glaser, "Studies of the Characteristics of Probable Lunar Surface Materials," Air Force Cambridge Research Laboratories, Special Report No. 20, January 1964.

4. A. E. Wechsler and I. Simon, "Thermal Conductivity and Dielectric Constant of Silicate Materials," Arthur D. Little, Inc., Contract No. NAS 8-20076, December 1966.

5. A. E. Wechsler and P. E. Glaser, "Thermal Conductivity of Non-Metallic Materials," Arthur D. Little, Inc., Contract No. NAS 8-1567, June 1964.

6. A. E. Wechsler and P. E. Glaser (1965), Icarus, 4, No. 4, P. 335-352.

7. E. C. Barnett, et al (1963), AIAA Journal, 1, 6, P. 1402.

8. Carslow and Jaeger, "Conduction of Heat in Solids," Oxford University Press, 1948.

9. Patterson, "The Conduction of Heat in a Medium Generating Heat," Philosophical Magazine, Volume 32, P. 384, 1941.

Table 1

Thermal Conductivity in Vacuum

LUNAR SOIL SIMULANT - TYPE A

Heater Power (watts)	Initial Temp. Kelvin	Range of Match Kelvin	Match Temp. T* °Celsius	Computed Temp. Kelvin	Thermal Conductivity K x 10^{-6} watts/cm °C
0.42	377.5	386.0 448.5	37.0	414.5	59.3
0.42	370.5	394.5 456.4	27.5	398.0	79.7
0.42	295.5	313.5 397.5	56.0	351.5	39.2
0.42	296.0	301.5 394.5	55.0	351.0	39.9
0.42	237.0	242.0 347.5	71.0	308.0	30.9
0.42	209.0	214.5 308.5	96.0	305.0	22.8
0.42	240.5	258.0 363.5	57.0	297.5	38.5
0.42	213.5	228.5 340.5	70.0	283.5	31.3
0.19	188.5	205.0 222.0	23.0	211.5	45.1
0.19	181.0	197.0 220.5	25.0	206.0	39.7

T* - See text paragraph 28

NOTE: See Figure 2 and paragraph 8 for Type A gradation.

Table 2

Thermal Conductivity in Vacuum

LUNAR SOIL SIMULANT - TYPE A-1

Heater Power (watts)	Initial Temp. Kelvin	Range of Match Kelvin	Match Temp. T* °Celsius	Computed Temp. Kelvin	Thermal Conductivity $K \times 10^{-6}$ watts/cm °C
0.42	392.5	442.5 507.5	50.0	442.5**	43.8
0.45	378.0	380.0 460.0	52.0	430.0**	45.1
0.42	383.5	401.5 460.5	42.0	425.5**	52.2
0.45	267.0	368.5 440.5	45.0	412.0**	52.5
0.435	325.5	333.5 406.0	53.0	378.5**	42.8
0.435	318.5	327.5 392.0	46.0	364.5**	49.3
0.42	277.0	279.5 376.0	71.5	348.5**	30.6
0.42	280.0	286.5 374.0	59.5	339.5	36.8
0.435	243.5	248.5 323.0	74.0	317.5	30.6
0.435	242.0	250.0 338.5	69.0	311.0	32.9
0.42	200.0	213.0 348.0	110.0	310.0	19.9

Table 2(Cont'd.)

Heater Power (watts)	Initial Temp. Kelvin	Range of Match Kelvin	Match Temp. T* ^{o}Celsius	Computed Temp. Kelvin	Thermal Conductivity K x 10^{-6} watts/cm ^{o}C
0.42	209.0	219.0 334.5	96.0	305.0	22.8
0.42	224.0	225.5 318.5	77.5	301.5	28.2
0.42	199.0	210.5 343.0	102.0	301.0	21.5
0.42	202.0	213.5 325.0	95.0	297.0	23.0
0.19	163.0	199.0 273.5	46.0	229.0	26.8
0.19	192.0	211.0 262.5	37.0	229.0	21.5
0.105	177.0	205.5 249.0	33.0	210.0	16.6
0.105	186.5	206.5 250.5	22.0	208.5	24.9

T* - See text paragraph 28.

** - These points were not used in the least squares fit of curve.

NOTE: See Figure 2 and paragraph 8 for Type A-1 gradation.

Table 3

Thermal Conductivity in Vacuum

LUNAR SOIL SIMULANT - TYPE A-2

Heater Power (watts)	Initial Temp. Kelvin	Range of Match Kelvin	Match Temp. T* °Celsius	Computed Temp. Kelvin	Thermal Conductivity K x 10^{-6} watts/cm °C
0.42	299.0	332.5 399.0	40.0	339.0	54.8
0.42	299.5	316.5 371.5	30.5	330.0	71.9
0.20	294.0	309.5 348.5	20.8	314.8	50.2
0.20	294.5	301.5 330.0	16.3	310.8	64.1
0.30	245.5	221.5 303.0	50.5	296.0	32.0
0.42	235.0	280.0 376.0	52.5	287.5	41.8
0.42	235.5	261.5 340.5	44.0	279.5	49.8
0.30	240.5	266.0 330.0	34.0	274.0	46.8
0.30	244.0	258.5 310.5	27.5	271.5	56.9
0.30	207.0	216.0 276.5	43.0	250.0	36.4
0.30	200.5	221.5 303.5	49.0	249.5	32.0
0.42	164.5	230.5 335.5	53.0	227.5	41.4
0.42	168.0	217.0 300.0	45.0	223.0	48.7

T* - See text paragraph 28

NOTE: See Figure 2 and paragraph 8 for Type A-2 gradation.

Table 4

Thermal Conductivity in Vacuum

LUNAR SOIL SIMULANT - TYPE A-3

Heater Power (watts)	Initial Temp. Kelvin	Range of Match Kelvin	Match Temp. T* °Celsius	Computed Temp. Kelvin	Thermal Conductivity K x 10^{-6} watts/cm °C
0.42	246.5	260.0 312.5	27.0	273.5	81.2
0.42	241.5	265.5 314.5	20.0	271.5	110.0
0.42	204.0	223.0 304.5	30.0	234.0	73.1
0.42	194.5	232.5 285.5	25.0	219.5	87.7
0.42	167.0	209.0 288.5	36.0	204.0	62.7
0.42	155.0	199.5 257.0	35.0	190.0	60.9

T* - See text paragraph 28.

NOTE: See Figure 2 and paragraph 8 for Type A-3 gradation.

Table 5

Summary of Conduction and Radiation
Contributing to Effective Thermal Conductivity

Model or Material	Bulk Density ($Kg\ m^{-3}$)	Temperature ^{o}K	Solid Conduction Contribution (watt/cm ^{o}C)x10^{6}	Radiation Contribution (watt/cm ^{o}C)x10^{6}	Total Effective Thermal Conductivity (watt/cm ^{o}C)x10^{6}	Ratio $\frac{\text{Radiation}}{\text{Conduction}}$
I* (40-149μ)	1350	200	17.7	2.64	20.34	0.149
		300	17.7	8.92	26.62	0.504
		400	17.7	21.15	38.85	1.195
II* (40-149μ)	1350	200	4.63	19.85	24.48	4.25
		300	-42.23	66.98	24.75	-1.59
		400	-89.08	158.76	69.68	-1.78
III* (40-149μ)	1350	200	17.72	2.63	20.35	0.148
		300	17.74	8.88	26.62	0.501
		400	17.76	21.05	38.81	1.185
Basalt** Powder (10-37μ)	1360	200	12.75	0.70	13.45	0.054
		300	15.37	2.38	17.75	0.154
		400	16.68	5.63	22.31	0.34
Basalt** Powder (44-74μ)	1430	200	6.14	1.71	7.85	0.28
		300	6.14	5.78	11.92	0.94
		400	6.14	13.70	19.84	2.24

*Mathematical models for Type A-1 material
**Thermal conductivity data from Wechsler and Simon (1966)

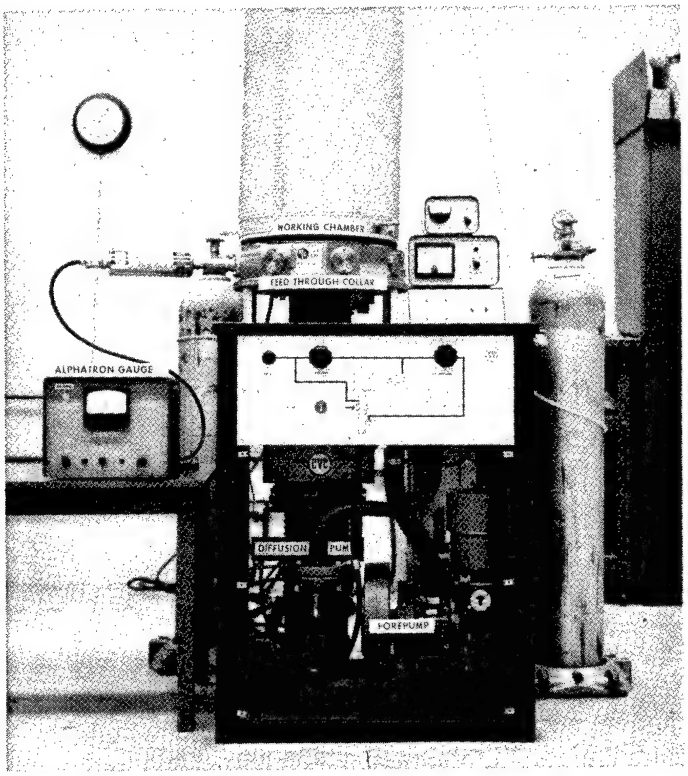

a. High Vacuum Facility - Front View

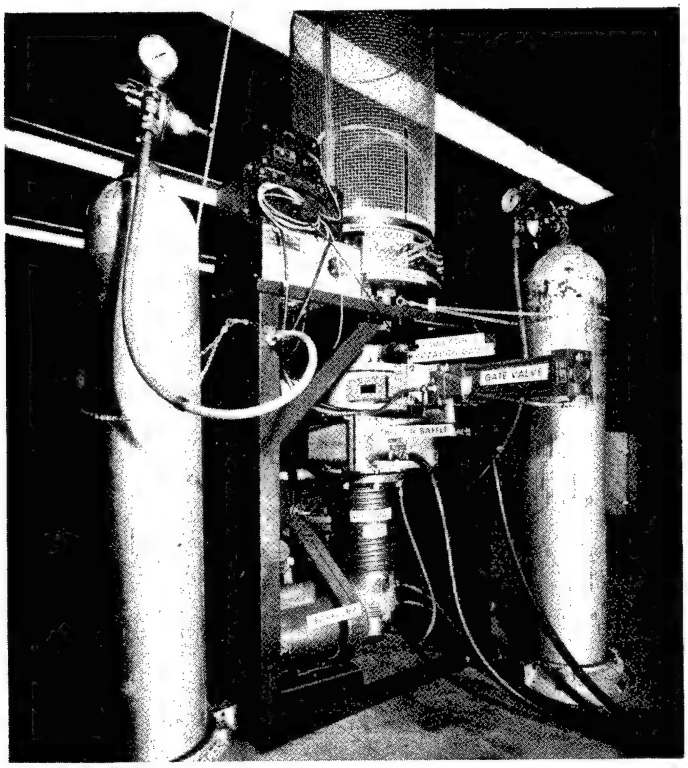

b. High Vacuum Facility - Rear View

Plate 1

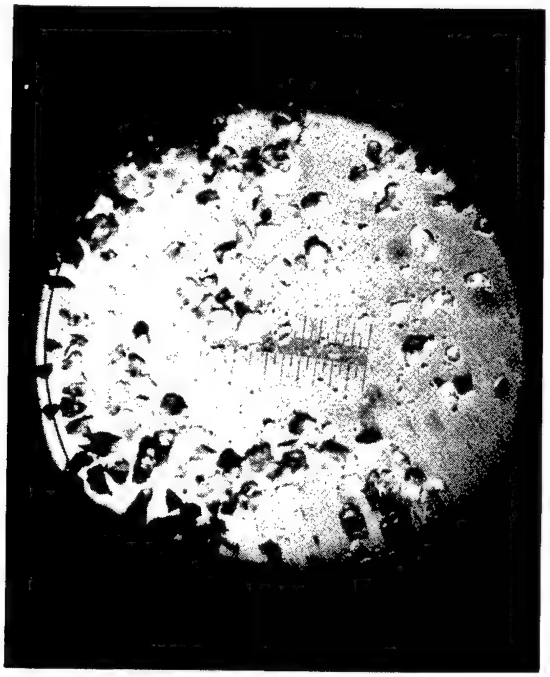

a. Photomicrograph of Type A-1 Material - 20X Nominal Magnification

b. Photomicrograph of Type A-1 Material - 40X Nominal Magnification

Plate 2

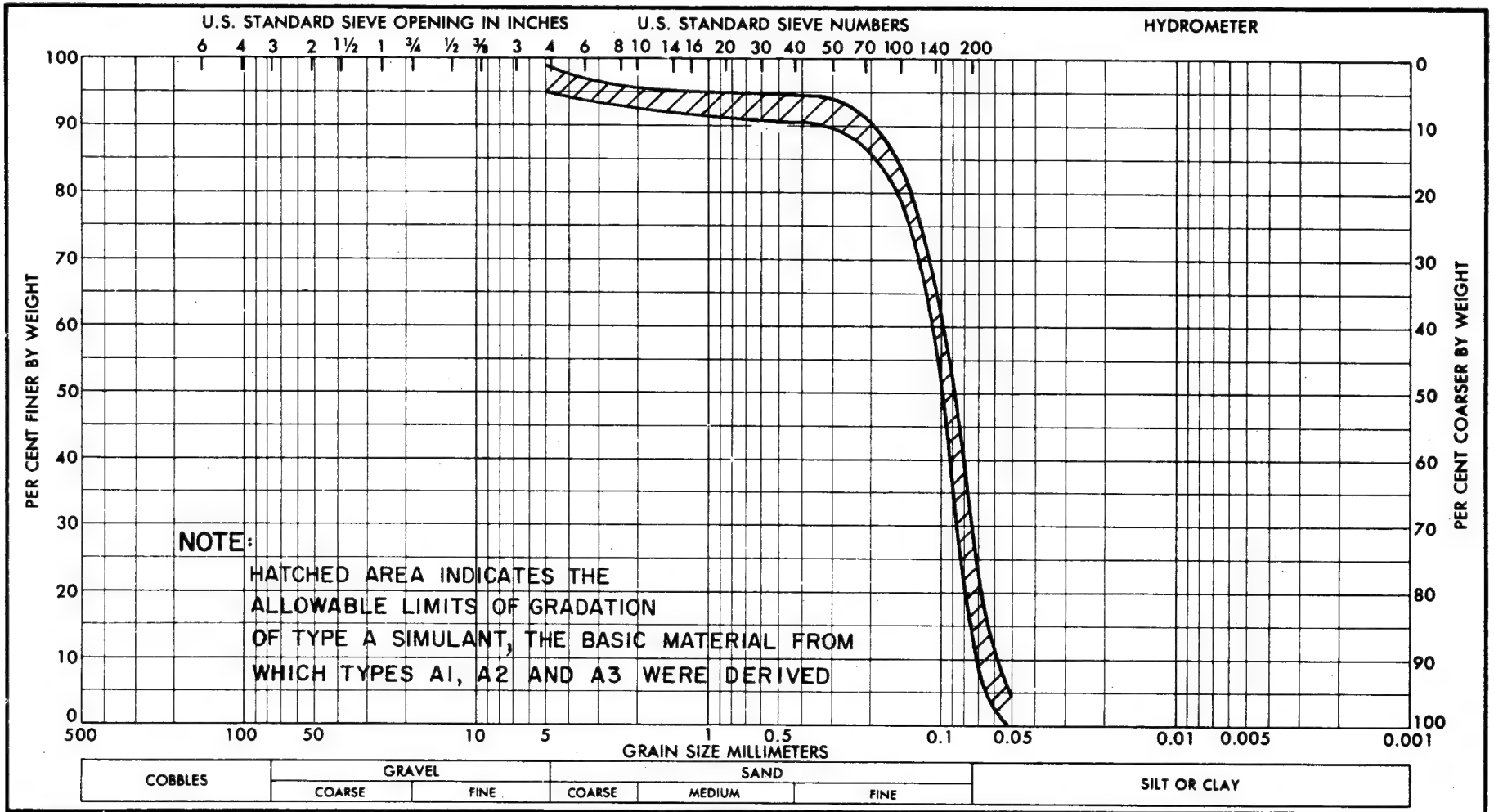

SAMPLE NO.	ELEV OR DEPTH	CLASSIFICATION	NAT W%	LL	PL	PI

GRADATION CURVES

PROJECT LUNAR SOIL SIMULANT
—TYPE A—
AREA LUNAR SOIL SIMULANT STUDY
BORING NO. PHASE B, PART 2
DATE

FIGURE 1

ENG FORM 2087
1 MAY 63

REPLACES WES FORM NO. 1241, SEP 1962, WHICH IS OBSOLETE.

U.S. GOVERNMENT PRINTING OFFICE : 1963 OF—709-126

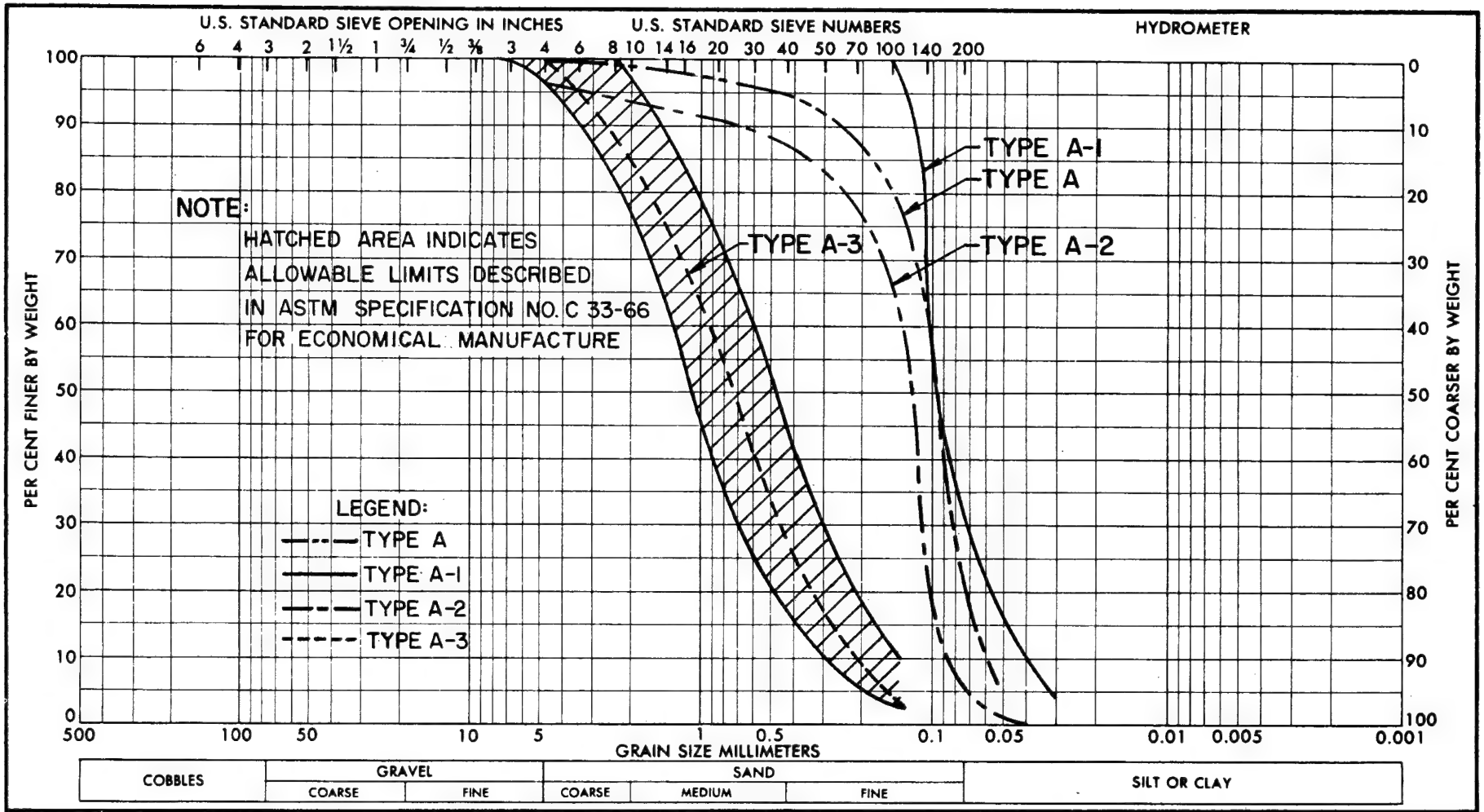

SAMPLE NO.	ELEV OR DEPTH	CLASSIFICATION	NAT W%	LL	PL	PI

GRADATION CURVES

PROJECT LUNAR SOIL SIMULANT STUDY

PHASE B, PART 2

AREA GRADATION FRACTIONS

BORING NO. OF BASIC SIMULANT

DATE

FIGURE 2

ENG FORM 2087
1 MAY 63

REPLACES WES FORM NO. 1241, SEP 1962, WHICH IS OBSOLETE.

U.S. GOVERNMENT PRINTING OFFICE : 1963 OF—708-126

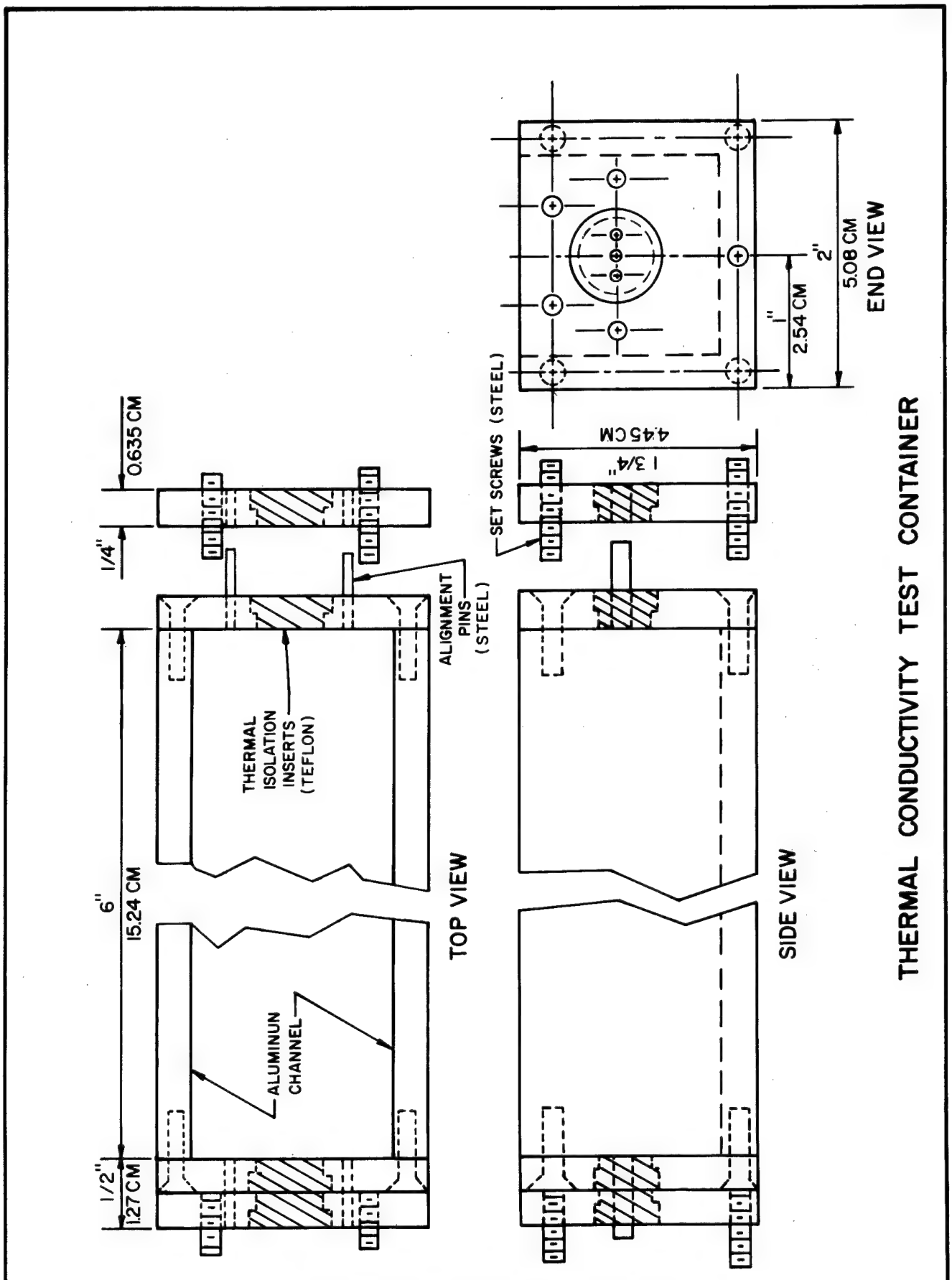

LUNAR SOIL SIMULANT STUDY
PHASE B, PART 2

FIGURE 3

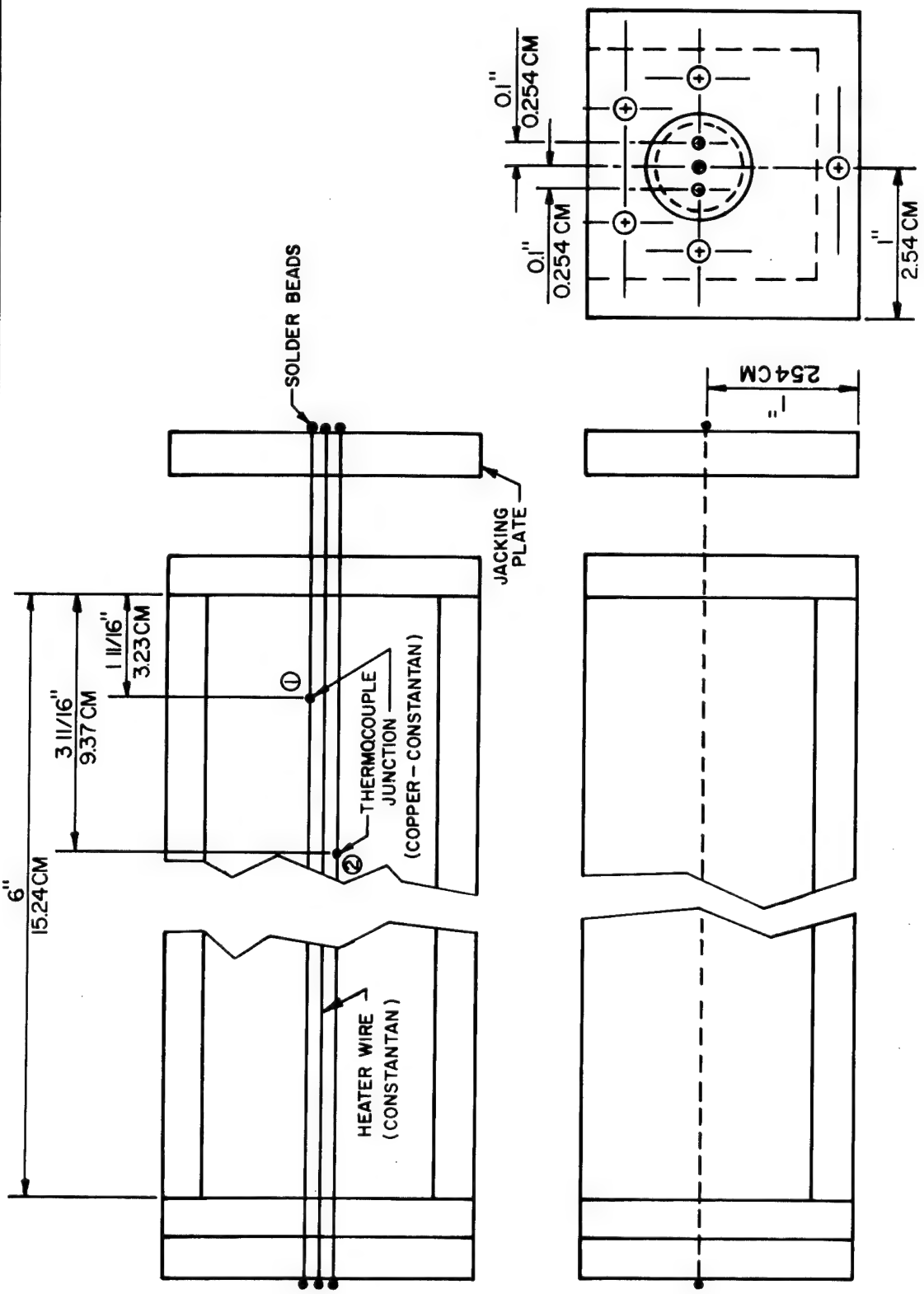

LAYOUT OF WIRES IN TEST CONTAINER
FOR THERMAL CONDUCTIVITY MEASUREMENTS

LUNAR SOIL SIMULANT STUDY
PHASE B, PART 2

FIGURE 4

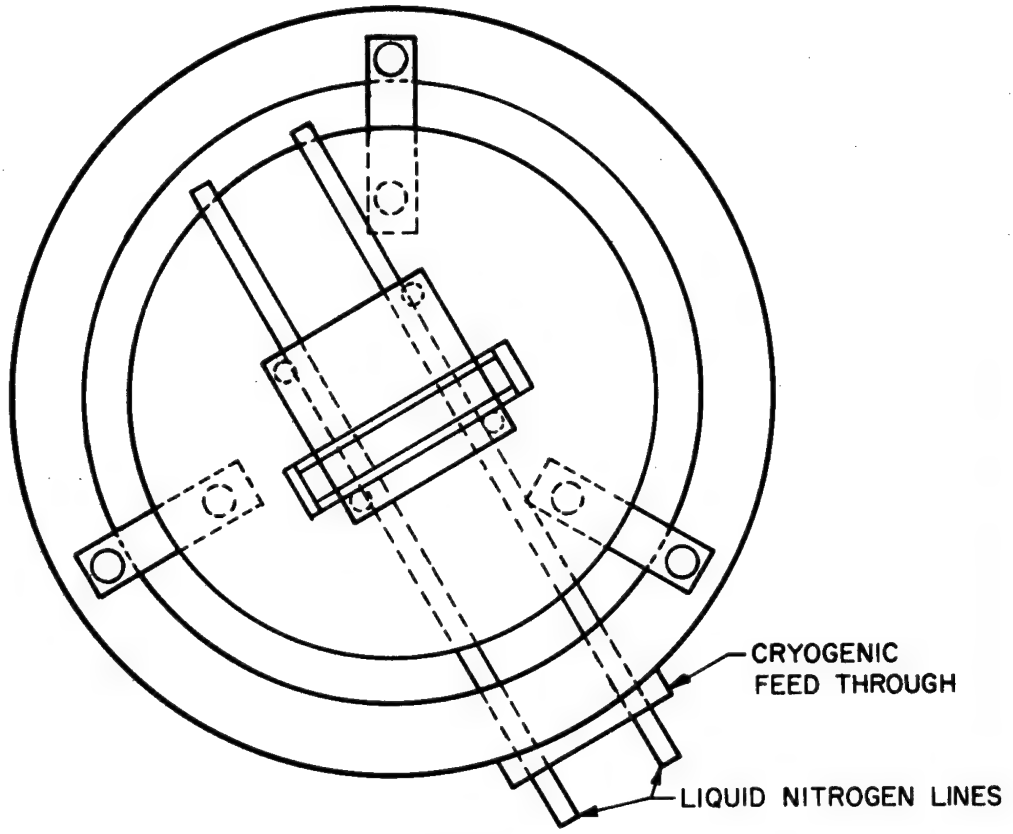

TOP VIEW

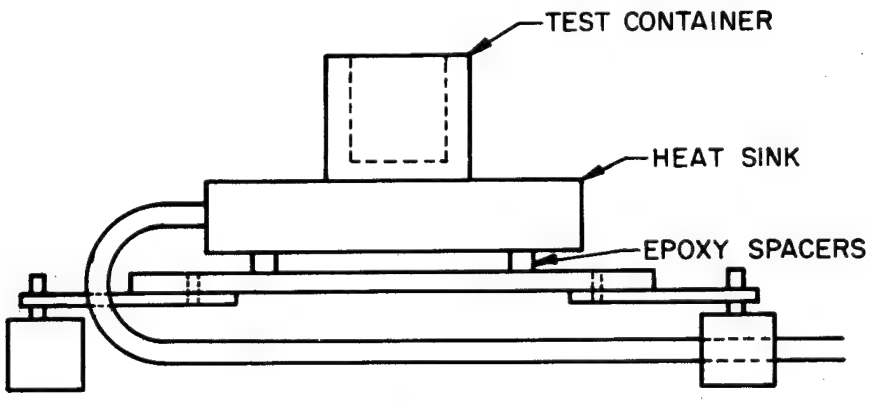

SIDE VIEW

SCHEMATIC LAYOUT OF TEST CONTAINER AND HEAT SINK

LUNAR SOIL SIMULANT STUDY

PHASE B, PART 2

FIGURE 5

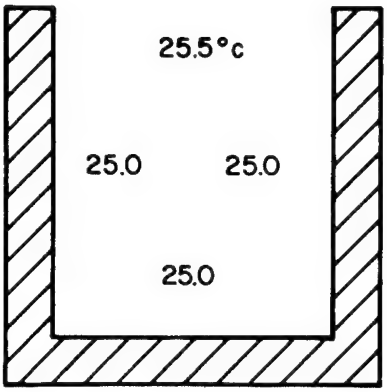

INITIAL TEMPERATURE
DISTRIBUTION

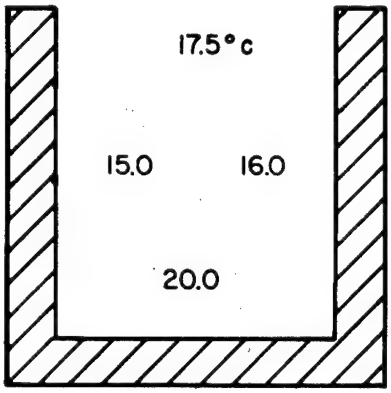

TEMPERATURE DISTRIBUTION
AFTER 25 MINUTES

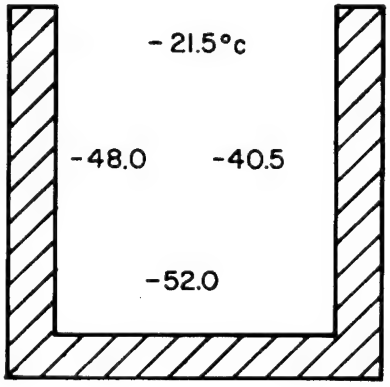

TEMPERATURE DISTRIBUTION
AFTER 60 MINUTES

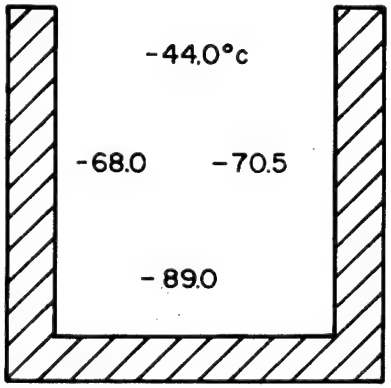

TEMPERATURE DISTRIBUTION
AFTER 90 MINUTES

TEMPERATURE GRADIENT WITHIN SAMPLE (DEGREES CELSIUS) FROM THERMOCOUPLE PROBE TESTS UNDER VACUUM

LUNAR SOIL SIMULANT STUDY

PHASE B, PART 2

FIGURE 6

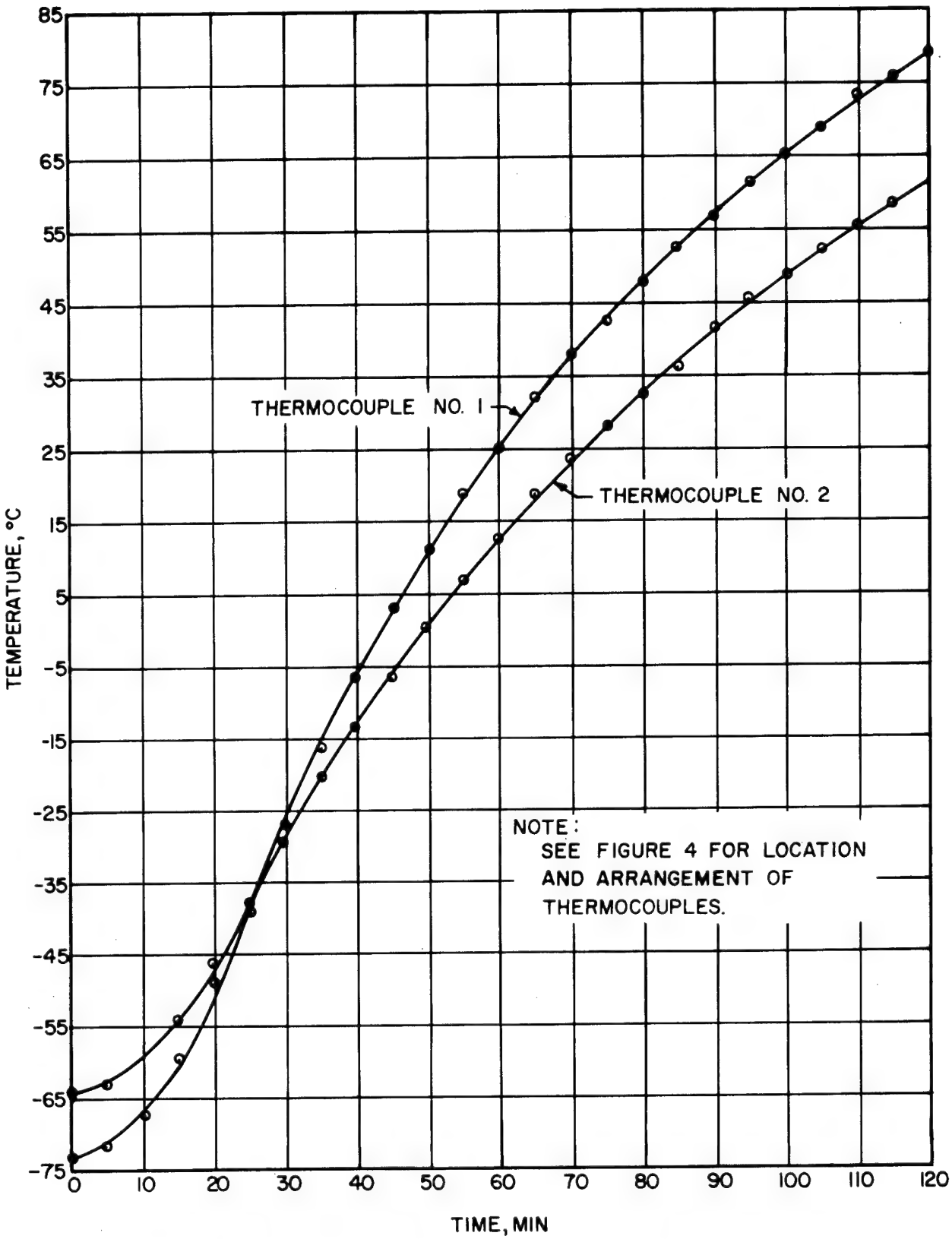

TYPICAL PLOTS OF TIME-TEMPERATURE MEASUREMENTS FOR TYPE A-1 MATERIAL AT 5×10^{-5} TORR

LUNAR SOIL SIMULANT STUDY

PHASE B, PART 2

FIGURE 7

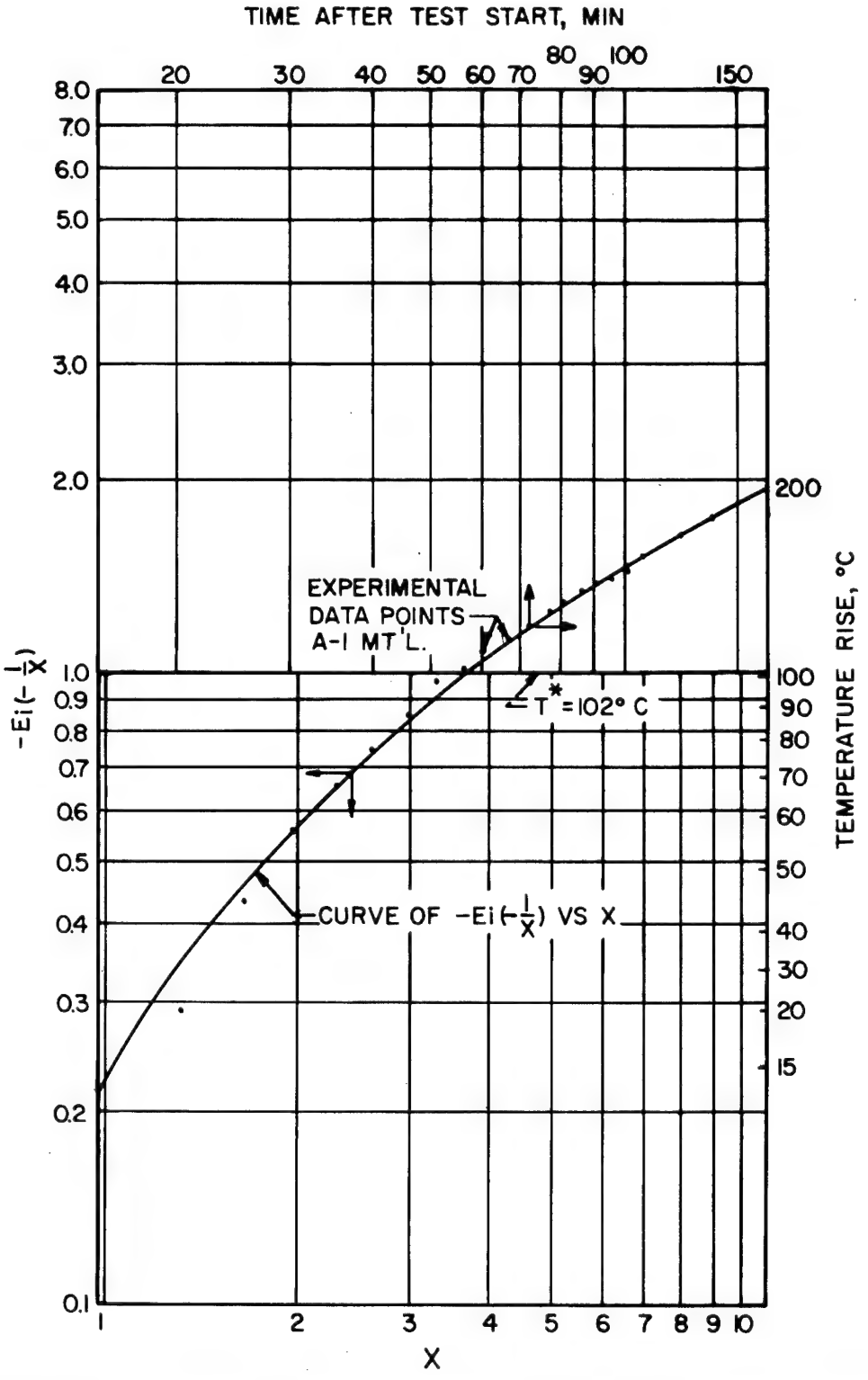

STANDARD CURVE AND TYPICAL EXPERIMENTAL POINTS FOR COMPUTATION OF THERMAL CONDUCTIVITY "K"

(SEE REFERENCE NO. 3 & 5)

LUNAR SOIL SIMULANT STUDY

PHASE B, PART 2

FIGURE 8

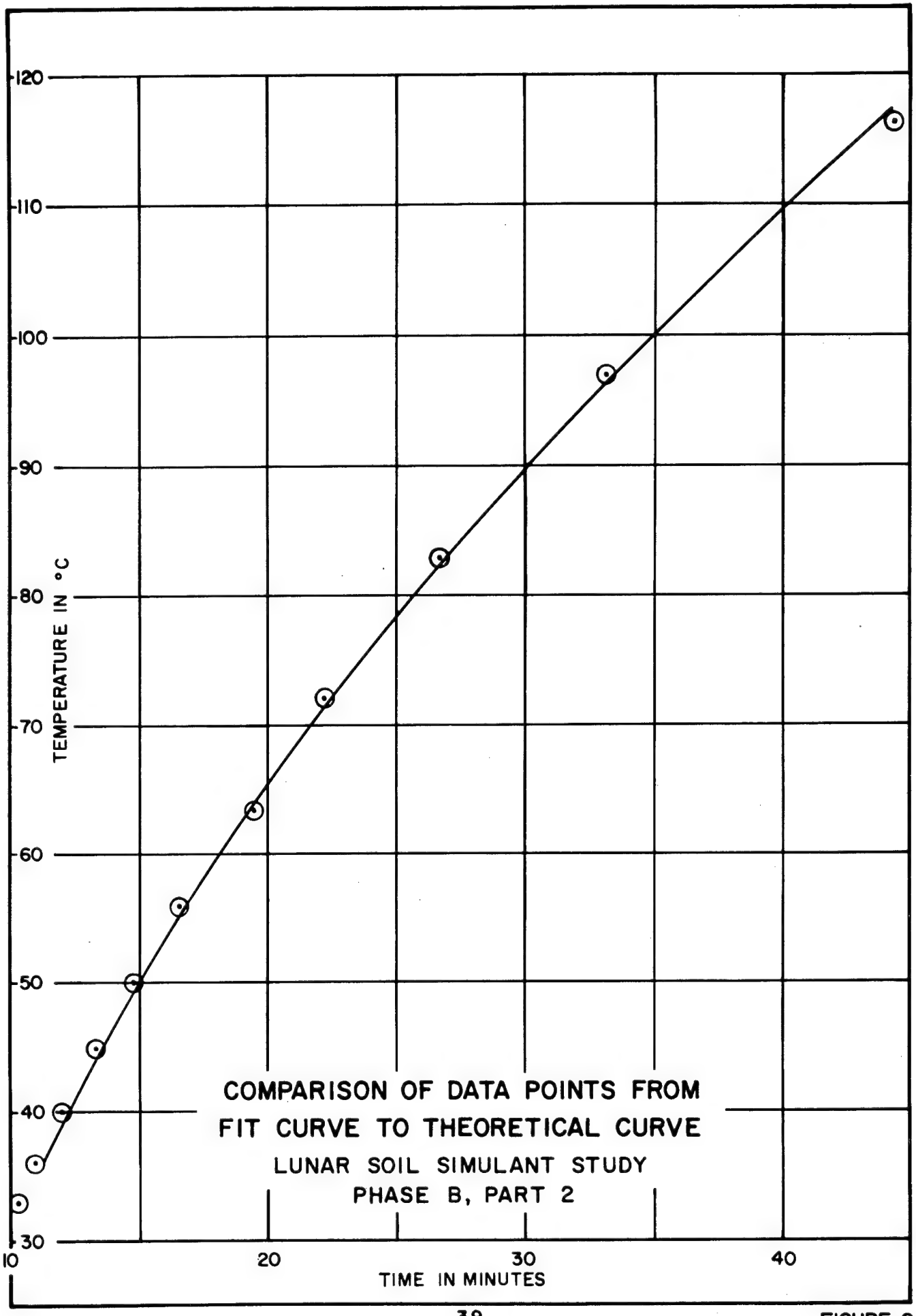
120
110
100
90
80
70
60
50
40
30
TEMPERATURE IN °C
10
20
30
40
TIME IN MINUTES
COMPARISON OF DATA POINTS FROM
FIT CURVE TO THEORETICAL CURVE
LUNAR SOIL SIMULANT STUDY
PHASE B, PART 2

FIGURE 9

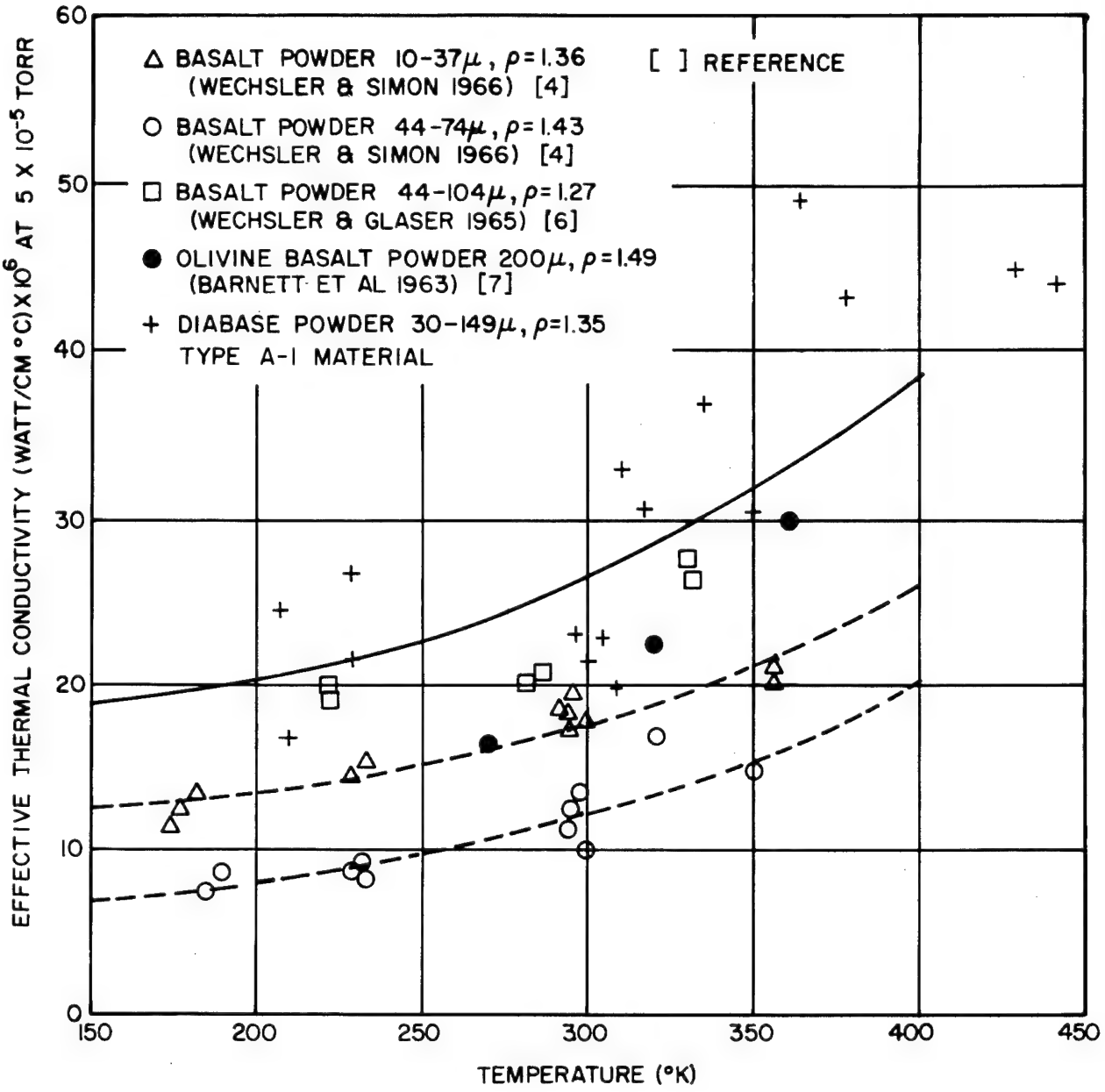

EFFECTIVE THERMAL CONDUCTIVITY VS
TEMPERATURES FOR FIVE BASALT POWDERS
LUNAR SOIL SIMULANT STUDY
PHASE B, PART 2

FIGURE 10

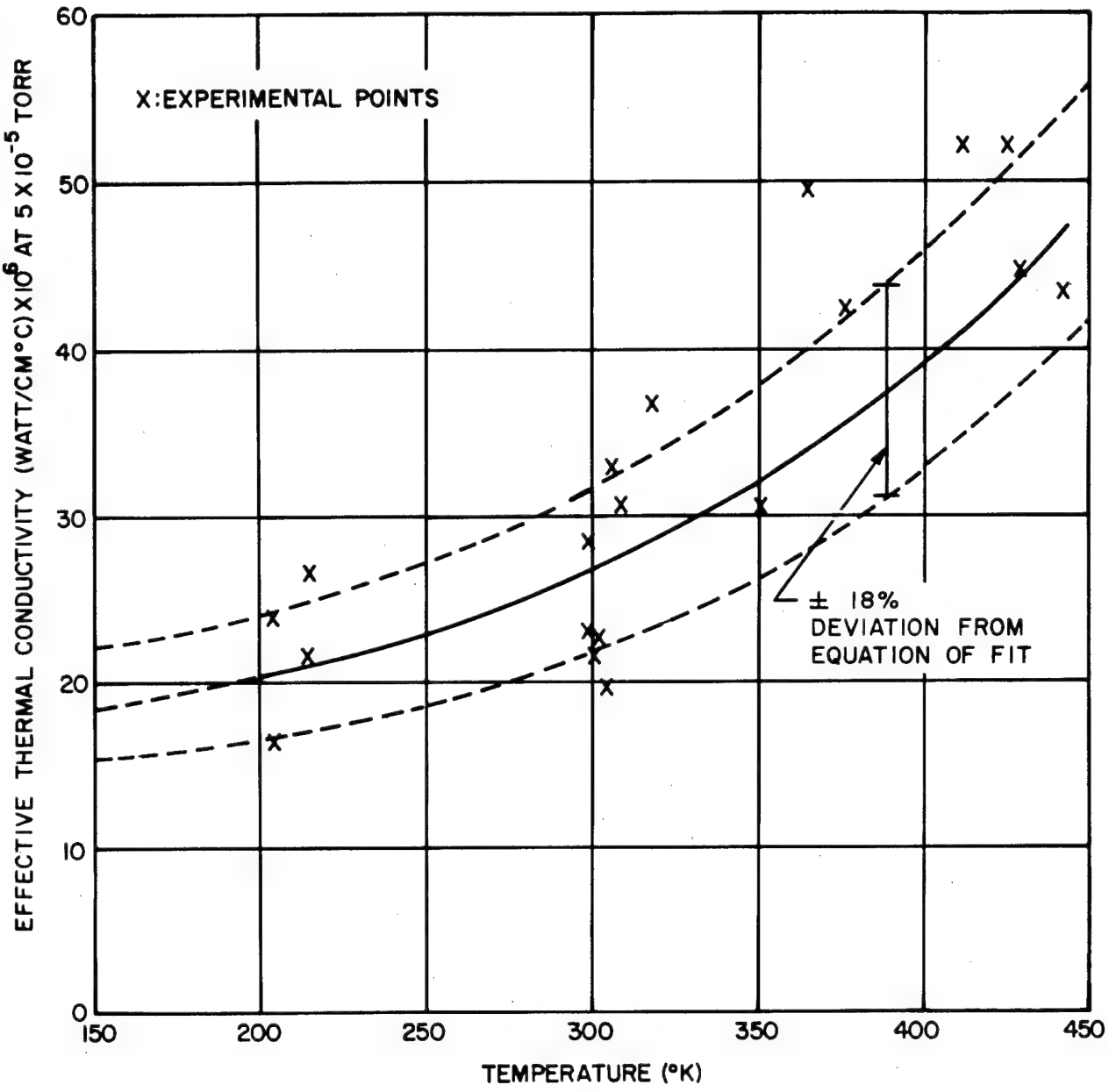

EFFECTIVE THERMAL CONDUCTIVITY VS
TEMPERATURE FOR TYPE A-1 LUNAR SOIL SIMULANT
SHOWING RMS DEVIATION

LUNAR SOIL SIMULANT STUDY
PHASE B, PART 2

FIGURE 11

APPENDIX A

Analysis of Error Associated with Test Boundary Conditions

68. Heat transfer from simulant to heat sink may have been significantly affected by the test container and its relation to the heat sink reservoir. The typical set of temperature readings presented on Figure 6 shows that a uniform temperature field was improbable for any test. The following analysis was completed in order to assess the effect of an initial temperature gradient on the determinations of thermal conductivity.

69. According to Carslow and Jaeger (8) the governing equation for the change in temperature with time for an infinite medium containing distributed sources of heat is:

$$\frac{\partial T}{\partial t} = \alpha \nabla^2 T + f(x, y, z, t) \qquad (4)$$

where f (x, y, z, t) is the rate of heat production per unit volume. The general case of the rate of heat generation not equal to zero consists of small finite regions of heat production bounded by regions of zero heat production. This means that the solution of equation (4) consists of the sum of two simpler solutions, i. e., the solution caused by the initial conditions and the solution caused by the source.

70. The continuous line heat source problem is a special case of the general equation when the heat generating function f (x, y, z, t) is confined to a line along one axis. By symmetry, the rate of change of the temperature along that axis is zero, and the problem reduces to a continuous point source in the plane normal to the axis.

71. Patterson (9) solved the general equation for the case of the heat distribution caused by a point source. The remainder of this discussion will center on the temperature distribution caused by the initial conditions. In this way, the effect of the initial conditions on the subsequent temperature at some specified point, under the action of the source, can be determined.

72. According to Carslow and Jaeger, the effect of the initial conditions alone is:

$$w(x,y,t) = \frac{1}{4\pi\alpha t} \int_{-\infty}^{\infty} \int_{-\infty}^{\infty} \phi(x^1, y^1) \exp \frac{-(x-x')^2 + (y-y')^2}{4\alpha t} dx' dy' \quad (5)$$

where x^1 and y^1 are variables of integration, and (x, y, t) is the point at which w is to be determined. In order to apply this relationship to the problem of this report, it will be necessary to use the following coordinate system:

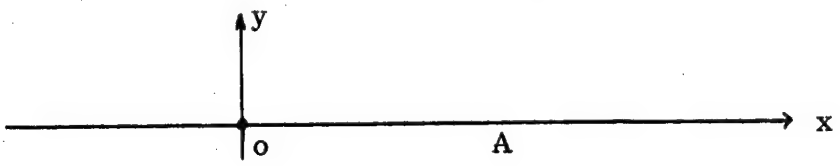

in which it is desired to determine the temperature at A caused by a source at o and an initial temperature distribution $\phi(x, y)$. Let the initial temperature distribution be linear in x and y as,

$$\phi = (a_o + k_1 x) + (b_o + k_2 y) \quad (6)$$

where k_1 and k_2 are chosen to approximate the initial temperature distribution, and a_o and b_o are arbitrary constants. The function ϕ represents the initial temperature measured above the starting temperature.

73. The solution of the source free part of equation (4) involves the initial conditions,

$$T = T(x, y, z, o) = \varphi(x, y, z) \quad (7)$$

$$= \phi_1(x, y, z) + \phi_2(x, y, z) \quad (8)$$

It can be shown, then, that the solution of the source free part is

$$T = T_1 + T_2 \quad (9)$$

where:

$$T_1(x, y, z, o) = \phi_1(x, y, z)$$
$$T_2(x, y, z, o) = \phi_2(x, y, z)$$

Only the source free solution caused by a particular initial temperature need be considered. For the experimental apparatus, it is approximately true (and

theoretically exactly true) that the initial temperature distribution along both the x and y axes is linear. This fact was verified experimentally by inserting a set of probes at various locations within the simulant and observing the temperature states over the entire temperature range (See Figure 6).

74. The next step in analysis is to consider the contribution to the complete solution given by a source solution with zero initial temperature distribution. Using equation (5) to describe the source free state, and superposing a linear temperature distribution in the x direction only (from equation 6), the solution to the basic differential equation is:

$$w(x, y, z, t) = \frac{1}{4\pi\alpha t} \int_{-\infty}^{\infty} \int_{-\infty}^{\infty} (b_o + k_2 y') \exp \frac{-(x-x')^2 + (y-y')^2}{4\alpha t} dx' dy' \qquad (10)$$

This reduces to:

$$w = \frac{1}{4\pi\alpha t} \int_{-\infty}^{\infty} b_o \exp \frac{-(x-x')^2}{4\alpha t} dx' \int_{-\infty}^{\infty} \exp \frac{-(y-y')^2}{4\alpha t} dy' + \qquad (11)$$

$$\frac{1}{4\pi dt} \int_{-\infty}^{\infty} \exp \frac{-(x-x')^2}{4\alpha t} dx' \int_{-\infty}^{\infty} k_2 y' \exp \frac{-(y-y')^2}{4\alpha t} dy'$$

In order to evaluate equation (11), substitute for a fixed y and x the change of variables

$$y - y' = p \qquad (12)$$

$$x - x' = -q$$

Equation (11) then becomes:

$$w = \frac{b_o}{4\pi\alpha t} \int_{-\infty}^{\infty} \exp\left(-\frac{q^2}{4\alpha t}\right) dq \int_{-\infty}^{\infty} \exp\left(-\frac{p^2}{4\alpha t}\right) dp + \qquad (13)$$

$$\frac{k_2}{4\pi\alpha t} \int_{-\infty}^{\infty} \exp\left(-\frac{q^2}{4\alpha t}\right) dq \int_{-\infty}^{\infty} (y+p) \exp\left(-\frac{p^2}{4\alpha t}\right) dp$$

Note that the second product in equation (13) vanishes when y = 0 because

$$\int_{-\infty}^{\infty} p \, e^{-\frac{p^2}{4\alpha t}} dp = 0$$

If the following substitutions are made in equation (13),

$$\beta = \frac{q}{\sqrt{4\alpha t}}; \quad \gamma = \frac{p}{\sqrt{4\alpha t}} \tag{14}$$

the equation reduces to:

$$w = \frac{b_o}{4\pi\alpha t} \int_{-\infty}^{\infty} e^{-\beta^2} (4\alpha t)^{1/2} \, d\beta \int_{-\infty}^{\infty} e^{-\gamma^2} (4\alpha t)^{1/2} \, d\gamma + (c) \; (y) \tag{15}$$

where c is a constant.

This equation is independent of t because the quantity $(4\alpha t)$ cancels and t does not appear in the integral.

75. The development just presented shows that for an initial linear temperature distribution in the y direction, the temperature at a given point is caused by the initial temperature distribution and will remain constant for all times. Hence, an initial linear temperature distribution has no effect on the computation of the thermal conductivity due to the impressed temperature changes due to a line source of heat. Clearly, an initial temperature gradient in the x direction leads to the same conclusion. It follows then that there is no uncertainty in results due to an initial linear temperature distribution.

APPENDIX B

Analysis of Error Implied by Data Analysis Technique

76. The basic equation associated with the line heat source method states that heat liberated by a line source at the rate q per unit time per unit length into a surrounding material at a uniform zero temperature will produce a temperature T at time t at a distance r from the heat source according to the equation:

$$T = \frac{-q}{4\pi k} \int_{r^2/4\alpha t}^{\infty} \frac{e^{-u}\,du}{u} \tag{16}$$

or

$$T = \frac{-q}{4\pi k} \; Ei \left(\frac{-r^2}{4\alpha t} \right) \tag{17}$$

Where:

Ei(x) = exponential integral of x

r = radial distance from line heat source (cm)

k = thermal conductivity of the media (cal/cm sec ^{o}c)

α = thermal diffusivity ($k/\rho\ c$) of the media (cal cc/g cm sec ^{o}c)

The assumptions inherent in the equation are discussed in Paragraphs 25 through 28.

77. Differentiation and rearrangement of the above equations result in the following equation which holds for an ideal line heat source at all times:

$$k = \frac{q}{4\pi} \frac{\left(t_1 \frac{dT}{dt}\right)^{b_1}}{\left(t_2 \frac{dT}{dt}\right)^{b_2}} \qquad (18)$$

where: $b_1 = \frac{t}{t_2 - t_1}$

$b_2 = \frac{t_2}{t_2 - t_1}$

t_1 and t_2 are any two different times

q = quantity of heat, (cal/cm sec)

t = time, (sec)

T = temperature, (^{o}K)

78. Analysis of the experimental results required fitting experimental data points with a polynomial curve derived by a statistical technique based on the least squares method. The fit obtained over a forty minute interval (with time as the independent variable) reduced to a parabola of the form:

$$t = c_1 + c_2 \; T + c_3 \; T^2 \qquad (19)$$

Differentiation of this curve yielded the slope $\frac{dT}{dt}$ for use in equation (18).

79. Assuming that the times are exact, the slopes $\frac{dT}{dt}$ are a source of error. For convenience, let $\frac{dT}{dt}$ equal ϕ. By definition, the relative error in the slope ϕ is $d\phi/\phi$, and in k is dk/k. To find an expression for the relative errors in each of these quantities, it is necessary to take the natural logarithm of equation (18) and differentiate the resulting expression to obtain:

$$dk = b_1 \left(\frac{d\phi_1}{\phi_1}\right) - b_2 \left(\frac{d\phi_2}{\phi_2}\right) \qquad (20)$$

80. The errors $d\phi$ are due to both the curve fitting technique and the experimental error in temperature measurement. Errors due to the curve fitting technique may be estimated by comparing the fit curve with the exact theoretical

curve expressed by equation (17). This is done by assuming typical values for the constants, r, k, α and q and computing an exact curve using equation (17). Points from this computation are then assumed to be experimental data points to which the statistical curve fitting technique applies. If the resulting fit curve correlates with the exact curve within the estimated experimental error, or at least nearly so, then the approximating curve may be considered as a smooth curve exactly representing the data. The errors in k and φmay then be estimated by comparing the smoothed curve with the exact curve.

81. The use of the theoretical curve was necessary to evaluate the error inherent in the curve fitting technique since there is no other standard with which to compare this method's accuracy. The constants assumed for the calculation of the exact curve were:

$$r = 0.2 \text{ cm}$$

$$\alpha = 2.5 \times 10^{-5} \text{ cm}^2/\text{sec}$$

$$k = 7 \times 10^{-6} \text{ cal/cm sec } ^{o}\text{C}$$

$$q = 0.007 \text{ cal/cm sec}$$

Evaluation of the exponential integral (equation 17) for these assumed constants yielded the set of points shown on Figure 9. These points were then considered to be experimental data to which a curve was fit using the least squares method with the aid of an electronic digital computer. The fit curve was the parabola satisfying the equation

$$T = -.03546t^2 + 4.356t - 7.467 \qquad (21)$$

82. The amount of error associated with the least squares method requires the calculation (using equation 21) of the times corresponding to the exact curve temperatures. Table B-1 shows the direct comparison of these times with the times calculated using the exact equation (equation 17). All thermocouple readings were completed within +0.25 minutes of the time schedule. From the table below, it is clear that the accuracy of the curve fitting technique is within the time accuracy of recording the observations. Figure 9 shows how closely the exact and computed curves mesh. The close correlation indicates that the computed curve may be considered to be exact.

Table B-1

Comparison of Times for Exact and Fit Curves

Temp °C	Time from Exact Curve min	Temp from Fit Curve °C
32.75	10.26	33.49
36.16	11.11	36.55
40.06	12.12	40.12
44.55	13.33	44.30
49.76	14.82	49.30
55.90	16.67	55.29
63.20	19.05	62.64
72.07	22.22	71.81
83.10	26.67	83.48
97.30	33.33	98.32
116.54	44.45	116.09

83. The relative error in slope, $\frac{d\phi}{}$, requires the use of both the exact and the computed curves. Differentiation of equation (17) yields:

$$\frac{dT}{dt} = \phi = \left(\frac{q}{4\pi k t}\right) \exp \frac{-r^2}{4\alpha t} \qquad (22)$$

Differentiation of the fit curve (equation 21) yields

$$\frac{dT}{dt} = \phi = -.07092t + 4.356 \qquad (23)$$

The change in slope $d\phi$ is the difference in calculated slopes of each curve for a given temperature. The relative error is defined as that decimal obtained by dividing the difference in slope by the slope of the exact curve at the given point. Table B-2 presents the relative error in slope over a typical computational interval of 15 minutes.

Table B-2

Relative Error in Slope

Time Min	Temp ^{o}C	Slope Exact ^{o}C/min	Slope Fit ^{o}C/min	Relative Error in Slope
15	50.94	3.40	3.29	0.0324
16	54.27	3.27	3.22	0.0153
17	57.44	3.16	3.15	0.0030
20	66.18	2.85	2.94	0.0308
25	79.66	2.44	2.58	0.0588
30	90.02	2.12	2.23	0.0514

This indicates that the error associated with finding the slope of the fit rather than the exact curve is negligible.

84. Equation (20) defines the relative error in calculated thermal conductivity $\frac{dk}{k}$. The error in k is greatly magnified if the time interval over which computations are made is too small. This follows because the quantities b_1 and b_2 (Equations 18 and 20) become large as the time interval decreases. To help define an optimum time interval, equation (20) was solved at two given slopes for a variety of time intervals. Table B-3 summarizes these results. Although the tabulated relative errors do not show a true minimum value, a greater time interval would introduce uncertainties into the applicability of the basic mathematical model. A time interval of 15 minutes implies a temperature range of 30^{o} or less over which the thermal conductivity is assumed to be constant. The results of this study show that the thermal conductivity is not constant over the temperature range investigated. However, the magnitude of change is not great enough to invalidate the assumption that the thermal conductivity remains constant over a temperature range of $30^{o}C$ or less.

Table B-3

Relative Error in Thermal Conductivity

Time Range Minutes	Time Interval Minutes	Relative Error in Thermal Conductivity (k)
15-16	1	0.2188
15-20	5	0.2049
15-25	10	0.1822
15-30	15	0.1308

DISTRIBUTION LIST

Chief of Engineers
ATTN: ENGMC-ED 15
ATTN: Library
ATTN: ENGTL
Department of the Army
Washington, D. C. 20315

The Engineer School
Technical Information Branch
Archives Section (Building 270)
Fort Belvoir, Virginia 22060

Director
U. S. Army Engineering
Waterways Experiment Station
ATTN: Soils Division
ATTN: Library
P. O. Box 631
Vicksburg, Mississippi 39181

Each Division Engineer
U.S. Army Engineer Division
ATTN: Laboratory

Deputy Chief of Staff for
Logistics, U. S. Army
The Pentagon
Washington, D. C. 20310

The Army Library
Office of the Adjutant General
The Pentagon, Room 1A530
Washington, D. C. 20315

Chief of Staff, United States Air Force
ATTN: Director of Civil Engineering,
DCS/P&R
AFOCE-KA
AFOCE-KC
Washington, D. C. 20330

Chief, Naval Facilities
Engineering Command
ATTN: Chief Engineer
Department of the Navy
Washington, D. C. 20350

Commanding General
U. S. Army Materiel Command
ATTN: AMCRD-T 2
Washington, D. C. 20315

Director
U.S. Army Cold Regions Research
and Engineering Laboratory
ATTN: AMXCR-EC
P. O. Box 282
Hanover, New Hampshire 03755

Director
U. S. Army Construction
Engineering Research Laboratory
Champaign, Illinois 61820

Each Division Engineer
ATTN: Library
ATTN: Chief, Engineering Division

Each District Engineer
U. S. Army Engineer District
ATTN: Library
ATTN: Chief, Engineering Division

Assistant Chief of Staff for
Intelligence, U. S. Army
The Pentagon
Washington, D. C. 20310

Commander-in-Chief
U. S. Army, Europe
APO New York, New York 09403

Director
Air Force Weapons Laboratories
ATTN: WLDC
Kirtland Air Force Base
New Mexico 87117

Chief, Naval Operations, Department
of the Navy
ATTN: The Library
Washington, D. C. 20360

Officer-in-Charge
U. S. Naval Civil Engineering Research and Evaluation Laboratory
Construction Battalion Center
Port Hueneme, California 93041

Commander, Air University
ATTN: Department of the Air Force Library
Maxwell Air Force Base,
Alabama 36112

Commander, USAF Institute of Technology
Wright-Patterson Air Force Base
Ohio 45433

Highway Research Board
National Research Council 3
2101 Constitution Avenue
Washington, D. C. 20418

Superintendent of Documents
Division of Public Documents
U. S. Government Printing Office
Washington, D. C. 20402

Building Research Advisory Board
National Academy of Sciences
2101 Constitution Avenue
Washington, D. C. 20418

Defense Documentation Center
ATTN: ENGAS-1
Caneron Station 20
Alexandria, Virginia 22315

Commander, Air Force Technical School
ATTN: Library
Francis E. Warren Air Force Base, Wyoming 82001

Commander, Civil Engineering Center
ATTN: AFIT-L Bldg. 640
Wright-Patterson Air Force
Ohio 45433

Engineering Scoieties Library
345 East 47th Street
New York, New York 10017

Library of Congress
Exchange and Gift Division
ATTN: American and British 2
Washington, D. C. 20540

Eleven (11) copies to: Chief of Engineers, Department of the Army
ATTN: ENGTE-AS
Washington, D. C. 20315

For Forwarding to:

Commander, Army Staff
British Joint Services Mission
Main Navy Building
Washington, D. C. 20360 5

Canadian Liaison Officer
c/o Engineer Research and Development Laboratories
ATTN: Secuirty Officer
Fort Belvoir, Virginia 22060 2

Canadian Joint Staff
2450 Massachusetts Avenue, N. W.
Washington, D. C. 20008 2

Chief, Construction Engineer
Air Service Branch, Department of Transport
Ottawa, Ontario, Canada

Mr. R. F. Legget
Division of Building Research
National Research Council of Canada
100 Suffex Drive
Ottawa, Ontario, Canada

DOCUMENT CONTROL DATA - R & D

(Security classification of title, body of abstract and indexing annotation must be entered when the overall report is classified)

1. ORIGINATING ACTIVITY *(Corporate author)*
U. S. Army, Corps of Engineers
Construction Engineering Laboratory
Ohio River Division Laboratories

2a. REPORT SECURITY CLASSIFICATION
Unclassified

2b. GROUP

3. REPORT TITLE
LUNAR SOIL SIMULANT STUDY, Phase B
PART II - THERMAL CONDUCTIVITY

4. DESCRIPTIVE NOTES *(Type of report and inclusive dates)*
Final Report

5. AUTHOR(S) *(First name, middle initial, last name)*
J. H. Hubbard
E. S. Gall
H. S. Kahn

6. REPORT DATE
May 1969

7a. TOTAL NO. OF PAGES
54

7b. NO. OF REFS
9

8a. CONTRACT OR GRANT NO.

b. PROJECT NO.

c.

d.

9a. ORIGINATOR'S REPORT NUMBER(S)
Technical Report 4-83

9b. OTHER REPORT NO(S) *(Any other numbers that may be assigned this report)*
See DDC number on cover

10. DISTRIBUTION STATEMENT
This document has been approved for public release and sale; its distribution is unlimited.

11. SUPPLEMENTARY NOTES

12. SPONSORING MILITARY ACTIVITY
DEPARTMENT OF THE ARMY

13. ABSTRACT

This report presents the results of an investigation into the thermal conductivity of a Lunar Soil Simulant at pressure levels of 5×10^{-5} torr and below. Thermal measurements were completed in vacuum over the temperature range of 200°K to 425°K. The Lunar Soil Simulant consisted of quarried diabase rock crushed and processed to the gradation of a fine sand. Four distinct combinations of the size fractions of this material permitted evaluation of the effect of grain size on the measurement of thermal conductivity within the sample container. This experimental data was correlated with data obtained by other investigations.

DD FORM 1 NOV 65 1473 REPLACES DD FORM 1473, 1 JAN 64, WHICH IS OBSOLETE FOR ARMY USE.

14. KEY WORDS	LINK A		LINK B		LINK C	
	ROLE	WT	ROLE	WT	ROLE	WT
Vacuum technology						
Lunar soil simulant						
Thermal conductivity						
Diabase rock						